Master's thesis

NTNU
Norwegian University of Science and Technology

Henrik Helland

Modelling and Optimization of a Solar Organic Rankine Cycle

Master's thesis in Energy and Environmental Engineering
Supervisor: Truls Gundersen
June 2019

NTNU
Norwegian University of
Science and Technology

Henrik Helland

Modelling and Optimization of a Solar Organic Rankine Cycle

Master's thesis in Energy and Environmental Engineering
Supervisor: Truls Gundersen
June 2019

Norwegian University of Science and Technology

NTNU
Kunnskap for en bedre verden

Abstract

To overcome the increasing energy demand and the problems associated with conventional methods of energy generation, sustainable and efficient methods must be developed. One of the solutions to the problem is solar-powered organic Rankine cycles (SORCs). Due to solar intermittency, most solar power plants incorporate thermal storage of energy. The stored energy is usually released in hours of high demand, resulting in power cycles operating with varying power outputs. In an attempt to increase the efficiency, the thermal storage could instead be used to distribute the power throughout the day evenly.

This thesis proposes a model of a SORC incorporating thermal storage to deliver constant power output. The model consists of a parabolic trough collector (PTC) with a two-tank direct sensible storage. A heat transfer fluid (HTF) is used to transfer heat between the collector and the organic Rankine cycle (ORC), via the storage tanks. Through simulation-based optimization using Matlab and HYSYS, the optimal operating conditions for the highest constant net power output of the model was found for different cases. A basic and a recuperative configuration of the ORC was developed for the model, and their differences investigated.

By lowering the minimum approach temperatures in the heat exchangers, higher efficiencies were obtained. The impact of this was greater for the recuperative ORC compared to the basic configuration. However, the introduction of the recuperator increases the mass flow rates of the HTF significantly.

The effects of different organic working fluids were also investigated. Ethylbenzene proved to be the best alternative for the recuperative ORC. For the basic ORC, however, toluene performed the best. Findings indicate that especially for the recuperative ORC, efficiencies increase with increasing molar mass.

The performance of the system is mainly dependent on the efficiencies of the ORC and the solar collector. The results of the optimization, however, suggests that the ORC efficiency is the most critical for achieving maximum power output.

Sammendrag

For å overvinne det økende energibehovet og problemene assosiert med konvensjonelle metoder for energigenerering, må bærekraftige og effektive metoder utvikles. En av løsningene på problemet er sol-drevene organiske Rankine-sykluser (SORC). På grunn av solens periodevise natur, benyttes termisk lagring av energi i de fleste solenergianlegg. Den lagrede energien frigjøres vanligvis i timer med høy etterspørsel, som resulterer i kraftsykluser som opererer med varierende levert effekt. I et forsøk på å øke virkningsgraden, kunne isteden det termiske lageret bli brukt til å levere stabil effekt gjennom hele dagen.

Denne oppgaven foreslår en modell av en SORC som benytter seg av termisk lagring for å levere konstant effekt. Modellen består av en parabolsk solfanger (PTC) med et totank direkte, følbart lager. En varmeoverføringsvæske (HTF) brukes til å overføre varme mellom solfangeren og den organiske Rankine-syklusen (ORC), via lagringstankene. Gjennom simuleringsbasert optimering ved bruk av Matlab og HYSYS, ble de best mulige arbeidsforholdene for høyest mulig effekt funnet for forskjellige scenarier. En grunnleggende ORC og en regenererende ORC ble utviklet til modellen, og forskjellene ble undersøkt.

Ved å senke de minste tilnærmingstemperaturene i varmevekslerne, ble høyere effektivitet oppnådd. Utslaget var større for den regenererende ORC-en sammenlignet med den grunnleggende konfigurasjonen. Imidlertid øker den introduserte regeneratoren massestrømmen av HTF betraktelig.

Effektene av å bruke forskjellige organiske arbeidsmedier ble også undersøkt. Ethylbenzen viste seg å være det beste alternativet for den regenererende ORC-en. For den grunnleggende ORC-en fungerte imidlertid toluen best. Funn indikerer, spesielt for den regenererende ORC-en, at effektivitetene øker med økende molar masse.

Systemets ytelse er hovedsakelig avhengig av effektivitetene til ORC-en og solfangeren. Resultatene av optimaliseringen antyder imidlertid at ORC-effektiviteten er den mest kritiske for å oppnå maksimal effekt.

Preface

This thesis was written during the spring of 2019. It is the final delivery of the Master of Science (MSc) degree in Energy and Environmental Engineering at the Norwegian University of Science and Technology (NTNU) at the Department of Energy and Process Engineering (EPT) in Trondheim.

I would like to thank Truls Gundersen and Haoshui Yu for their guidance during the process of writing this thesis and for providing an informal, yet rewarding atmosphere during the weekly meetings.

Henrik Helland
Trondheim, June 25, 2019

Table of Contents

List of Tables

List of Figures

Nomenclature

Symbols

Δ	change in property
$\dot{n}$	molar flow rate, kmol/s
$\dot{m}$	mass flow rate, kg/s
$\dot{Q}$	heat flow, kJ/s
$\dot{W}$	power, kW
η	efficiency, %
ac	aperture area, m^2
c_p	specific heat capacity, J/K · kg
g	gravitational acceleration, m/s^2
G_b	solar beam radiation, W/m^2
H	pump pressure head, m
h	specific enthalpy, kJ/kg
m	mass, kg
p	pressure, bar
Q	heat, kJ
S	entropy, kJ/K
s	specific entropy, kJ/kg· K
T	temperature, K, °C

W	work, kJ

Subscripts

$1, 2, 3, 4, 5, 6, 7, 8, 9, 10$	state/point
am	ambient
c	solar collector
$cond$	condenser
$cool$	cooler
el	electric
$evap$	evaporator/evaporation
min	minimum
rec	recuperator
s	isentropic
ts	time step

Abbreviations

CPC	compound parabolic collector
CSP	concentrated solar power
DNI	direct normal irradiation
EOS	equation of state
HC	hydrocarbon
HFC	hydrofluorcarbon
HTF	heat transfer fluid
LFC	linear Fresnel collector
LHS	latent heat storage
ORC	organic Rankine cycle
PCM	phase change material
PDR	parabolic dish reflector
PR	Peng-Robinson
PSO	particle swarm optimization

PTC	parabolic trough collector
PV	photovoltaic
SCT	solar central tower
SES	sensible heat storage
$SORC$	solar organic Rankine cycle
TES	thermal energy storage
THS	thermochemical heat storage

Chapter 1

Introduction

1.1 Background and Motivation

As the energy demand across the globe is rapidly increasing, the problems associated with conventional power generation are becoming more and more apparent. As a result of this, the need for environmentally friendly and efficient technologies are in increasing demand. A common problem among the so-called green energy sources, such as solar and wind, is that their availability varies throughout the day. This means that energy generation becomes highly uncontrollable. To counter this, the implementation of energy storage allows for more predictable systems. The stored energy will enable distribution in hours of high demand or delivery over extended periods, increasing the time spent generating while lowering the power output.

Solar energy technologies for electricity production has proven to be a viable option for green energy production. Today almost every new solar power plant utilizes thermal storage in combination with a power cycle to produce electricity. The peak hours of solar irradiation is usually in hours of low electricity demand in the grid. Because of this, thermal storage is generally used to store energy at peak solar hours, releasing it in hours of higher electricity demand and lower solar availability. As a result of this, the solar power plant usually is operating off-design conditions, reducing the efficiency of the power generation process.

The energy collected from the sun must be converted into mechanical power before it can be utilized to generate electricity. Several power cycles can be used in combination with solar energy. The most versatile and common cycle for this purpose, however, is the organic Rankine cycle (ORC). Although the conventional steam Rankine cycle dominates in terms of efficiency for heat sources at temperatures of 400°C or higher, these temperatures are out of reach for many conventional solar collector technologies.

1.2 Problem Description

The main objective of this master thesis project is to develop a model describing a solar organic Rankine cycle with constant power output. The model should include thermal storage and be modeled using software such as Matlab and Aspen HYSYS. The complete system model can then be used to find the optimal operating conditions through simulation-based optimization.

1.3 Scope

The main task of this thesis is to develop a model of a solar organic Rankine cycle that is to be optimized for the highest possible constant power output. The following sub-tasks follows from the main task and are accomplished using the optimization model:

- Compare of the optimized model to appropriate references.
- Investigate the effects of efforts to increase the power output.
- Investigate the effects of different working fluids in the organic Rankine cycle.

The following aspects of solar organic Rankine cycles are not considered:

- Loss mechanisms related to thermal storage.
- Heat and pressure loss in heat exchangers.
- Economic aspects.
- Environmental aspects of the organic working fluid.
- Safety aspects of the organic working fluid.
- Potential incompatibility between fluids and materials in the system.

1.4 Limitations

There are certain limitations when approaching the objective of this thesis. There is given a time limit of 20 weeks to complete the thesis. Matlab is a standard tool for students in the Energy and Environment study program and was chosen for the modelling of the solar collector and the heat storage. The author had no prior experience with Aspen HYSYS before the start of the project. The software was chosen despite this because of its ability to simulate organic Rankine cycles and compatibility with Matlab. The projects co-supervisor, Haoshui Yu, had applied simulation-based optimization using Matlab and HYSYS in his research and provided guidance.

The solar collector and thermal storage were modelled as a perfect system, meaning that there are no losses between the solar collector and the ORC. The efficiency of the solar collector is included. Challenges related to the interaction between Matlab and HYSYS

halted the development of more advanced models describing loss mechanisms more accurately. This results in much higher system efficiencies than what could be expected in real life. The case is the same for the heat exchangers in the ORC. However, isentropic, generator, and motor efficiencies are taken into account, meaning that the ORC efficiencies are more realistic. Consequently, only the ORC was compared directly to a reference model.

The proposed system model was optimized with different organic working fluids, four in total. They were only evaluated based on their performance under optimized conditions. Aspects that have been described as outside the scope of the thesis were not taken into account.

Data used as input parameters only describe the solar beam radiation and ambient temperatures for one particular day. Preferably other data sets should have been included. This was not done due to the time limitation and the accessibility of such data.

1.5 Report Structure

The report is divided into five main parts, presented in five chapters:

- Chapter 1: Introduces the problem description, main objectives, and the scope of the thesis.
- Chapter 2: Serves as a literature study, introducing the possibilities and relevant technologies for developing the model. This includes solar collector technologies, thermal storage technologies, and the organic Rankine cycle.
- Chapter 3: Describes the model developed, the assumptions made, and the optimization process.
- Chapter 4: Presents the results from the optimization of the proposed model. The results are discussed continuously as they are presented.
- Chapter 5: Concludes the report through the conclusion and suggestions for future work.

Chapter 2

Solar-Powered Organic Rankine Cycle

This chapter describes the main components of a solar organic Rankine cycle (SORC). Photovoltaic (PV) systems are also widely used in electricity generation, and the technology is well proven and mature. In later years, hybrid systems, combining concentrated solar power (CSP) and PV have been developed. Systems utilizing PV technology are, however, not discussed here.

2.1 Then and Now: Solar Power

The earliest accounts turning sunlight into work dates back to the ancient Greeks. The story of how Archimedes defended the city of Syracuse by using mirrors to concentrate the sunlight, igniting the incoming Roman ships, is well known, though the authenticity can be debated (Macchi and Astolfi, 2016). Nevertheless, the story describes some of the same technology as we deploy today when utilizing solar power.

The first European parabolic trough solar power plant, the Andasol-1, started operating in 2008. The plant, located in Granada, Spain, has a production capacity of 50 MW and covers a land area of 200 hectares, with a total aperture area for the collectors of 510,120 m^2. It is equipped with an indirect two-tank molten-salt storage system, capable of storing enough thermal energy to power the plant for 7.5 hours at full load. Powered by a steam Rankine cycle, the plant has a gross solar-to-electricity efficiency of 16 % (NREL, 2017)

2.2 Solar Irradiation

The content covered in section 2.2 is compiled from *"Solar Electricity"* by Markvart and Bogus (2000).

On average, the energy flux incident per unit area radiated from the sun perpendicular to the atmosphere of the earth is 1367 W/m^2. This is known as the solar constant (S) and represents the mean total solar irradiance. However, at a given point in time, solar radiation only hits an area of earth corresponding to disk ($A = \pi R^2$) with the same radius as the earth. Thus, by multiplying S with the area of this disk, and dividing by the earths total surface area ($A = 4\pi R^2$), one obtains the average flux incident per surface area unit on earth (S/4 = 342 W/m^2). However, this represents energy flux before it enters the atmosphere. When passing through the atmosphere, some of the energy is scattered or absorbed by air molecules, clouds, and particulate matter. The radiation that is scattered and still reaches the surface is called diffuse radiation. The radiation that passes through the atmosphere and reaches the surface directly from the sun is called beam radiation. Some radiation may also reflect from the surface onto another part of the surface. This is called the albedo.

2.3 Solar Thermal Collectors

The general concept of solar thermal technologies is to heat a heat transfer fluid (HTF) by utilizing the solar irradiation energy. Solar thermal collectors can generally be classified as either non-concentrating or concentrating collectors. Non-concentrating collectors absorb solar energy on the whole intercepting area, while the concentrating collectors reflect the irradiation on the intercepting area onto a smaller absorbing area (Tian and Zhao, 2013). Thus, the concentrating collectors are able to heat the HTF to much higher temperatures than the non-concentrating ones. In regions of the world with over 2500 annual sunshine hours, the concentrating collectors are preferred (Faninger, 2010).

2.3.1 Non-concentrating Collectors

The non-concentrating collectors can exploit all the radiation that reaches the collector. This means that the collectors can operate even under cloudy conditions when the diffuse part of the solar irradiation is dominating.

2.3.1.1 Flat Plate Collector

The flat plate collector is the most primitive and the most used solar collector (Pandey and Chaurasiya, 2017). It is made up by a transparent cover, absorber plates, insulation and tubes for the HTF. The transparent cover is usually made from sheets of glass which allows for high transmissivity of short-wave radiation and low transmissivity of long-wave radiation. This allows for the greenhouse effect to take place, as well as it reduces convection losses from the absorber plates. The purpose of the absorber plates is to absorb as much heat as possible. To achieve this, they are usually covered in dark materials. From

the absorber plates, the heat is transferred to the tubes containing the HTF. Different techniques have been applied to increase the heat transfer performance, for example, porous insertions in the tubes (Kumar and Reddy, 2009) and oscillating flow for the HTF (Lambert et al., 2006). The collector is cased in insulation to minimize the convection losses (Tian and Zhao, 2013). A flat plate collector is shown in Figure 2.1.

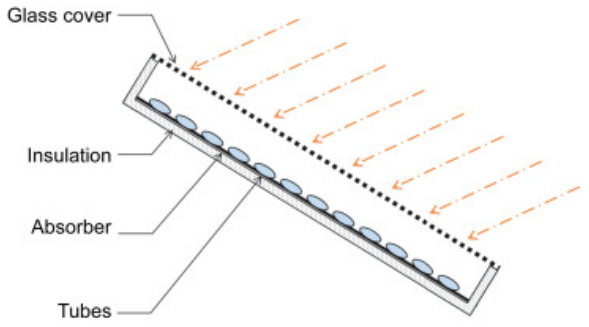

Figure 2.1: Flat plate collector (Orosz and Dickes, 2017).

Originally developed for hot water generation, the flat plate collector can be used, and is effective, for other applications at temperatures below 100 °C (Orosz and Dickes, 2017).

2.3.1.2 Evacuated Tube Collector

The evacuated tube collector is made up by two parallel glass tubes or pipes, one inside the other. The outer tube is transparent to allow irradiation to be absorbed by the inner tube, which is coated to allow for effective absorption. Between the two tubes, the air is sucked out to create a vacuum which insulates the inner tube. The HTF can be heated directly or indirectly: directly by flowing through the inner tube; indirectly by the use of an auxiliary HTF inside the inner tube. When using an auxiliary HTF, an evaporation-condensation cycle occurs in the tube, where it is evaporated by solar irradiation and condensed by the main HTF. The benefit of this indirect set-up is that the main HTF is heated to a constant temperature, regardless of the available irradiation (Orosz and Dickes, 2017). An evacuated tube collector with an auxiliary HTF is shown in Figure 2.2.

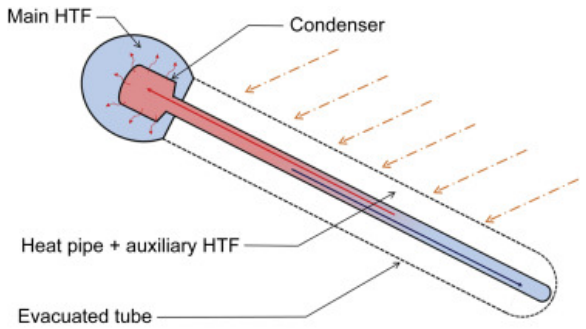

Figure 2.2: Evacuated tube collector (Orosz and Dickes, 2017).

For similar conditions, studies have found the evacuated tube collector to be more efficient than the flat plate collector (Sabiha et al., 2015; Ayompe et al., 2011). The evacuated tube collector can also achieve higher temperatures, with an operating range up to 150 °C (Orosz and Dickes, 2017).

2.3.2 Concentrating Collectors

The concentration ratio for concentrating collector is defined as the ratio between the aperture area and the area of the heat collector. For non-concentrating collectors, this ratio is 1, while for concentrating collector the ratio can be in the thousands. Due to their reflective nature, the concentrating collectors can only operate with beam radiation from the sun, also known as direct normal irradiation (DNI) (Orosz and Dickes, 2017).

2.3.2.1 Parabolic Trough Collector

The parabolic trough collector (PTC) transfers solar energy to the HTF by focusing the solar irradiation onto a receiver tube with flowing HTF. Parabolic shaped mirrors reflect the incoming irradiation onto a focal line, where the receiver tube is placed. This is usually done using glass mirrors, as they have a very high reflectivity (Steinhagen and Trieb, 2004). Because the sun moves across the sky during the day, tracking is required to ensure that the focal line hits the receiver tube. When installed correctly, it is only necessary to apply single-axis solar tracking to achieve this (Fernández-García et al., 2010). PTCs can achieve high concentration ratios, which allows the HTF to reach temperatures up to 400 °C (Orosz and Dickes, 2017). The PTC is the most prominent solar collector technology, being used in 71% of existing solar power plants (Tian and Zhao, 2013). The general design of a PTC is shown in Figure 2.3.

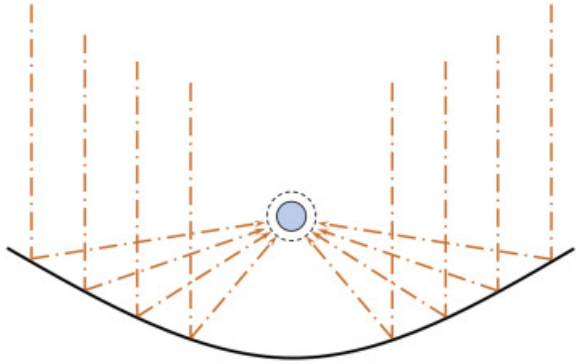

Figure 2.3: Parabolic trough collector (Orosz and Dickes, 2017).

2.3.2.2 Linear Fresnel Collector

The linear Fresnel collector (LFC) operates in a very similar fashion as the PTC. The difference is that the mirrors, or reflectors, are independent and flat instead of parabolic as they are for the PTC. This results in a cheaper system than the PTC, as flat reflectors are cheaper than parabolic. However, the concentration ratio is lower, which reduces the performance compared to the PTC (Morin et al., 2012). As for the PTC, the LFC is dependent on single-axis solar tracking to be efficient. The LFC is shown in Figure 2.4.

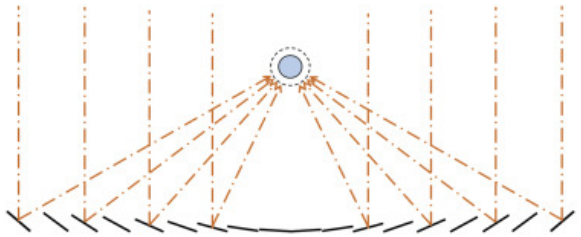

Figure 2.4: Linear Fresnel collector (Orosz and Dickes, 2017).

2.3.2.3 Compound Parabolic Collector

A compound parabolic collector (CPC) has a very similar design to the PTC. The main difference is the shape of the reflectors. They are designed in such a way that any irradiation entering the aperture area will be reflected onto the receiver tube, through internal reflections within the geometry (as shown in Figure 2.5). This eliminates the need for solar tracking, although the concentration ratio will be lower than for the PTC, and the achievable temperature is limited to around 200 °C (Orosz and Dickes, 2017).

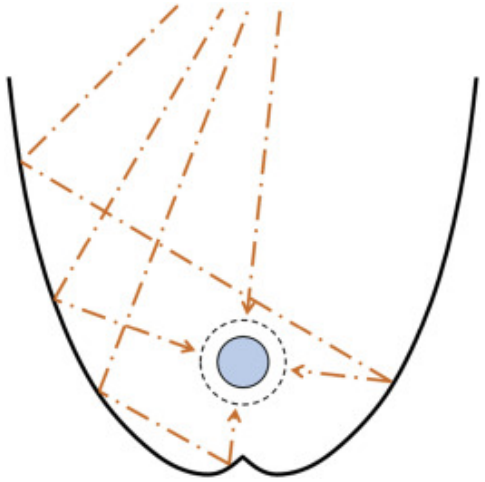

Figure 2.5: Compound parabolic collector (Orosz and Dickes, 2017).

2.3.2.4 Parabolic Dish Reflector

The parabolic dish reflector (PDR) is, as the name suggests, made up of a parabolic dish. The dish reflects the irradiation onto a single focal point (point-focus). The design is similar to the PTC (Figure 2.3), but instead of being stretched along one axis, it is revolved around the single focal point. A receiver is placed in the focal point to transfer the energy to the HTF. Because of its design, the PDR can achieve very high concentration ratios and temperatures (Chu and Meisen, 2011). In turn, this makes it more suitable for distributed systems for power generation, placing a heat engine directly at the focal point (Orosz and Dickes, 2017). It is therefore seldom used to heat an HTF for use in organic Rankine cycle (ORC) power plants. In addition, double-axis solar tracking is necessary to follow the motion of the sun throughout the day.

2.3.2.5 Solar Central Tower

A solar central tower (SCT) is, as the PDR, a point focus system. Reflectors, known as heliostats, focus incoming irradiation onto a receiver placed on top of a tower. These heliostats are dependent on double-axis tracking to stay focused on the receiver throughout the day (Collado and Guallar, 2013). SCTs can achieve high concentration ratios, which makes them well suited for high-temperature steam power plants, rather than for use in combination with ORCs (Orosz and Dickes, 2017). Figure 2.6 shows a SCT.

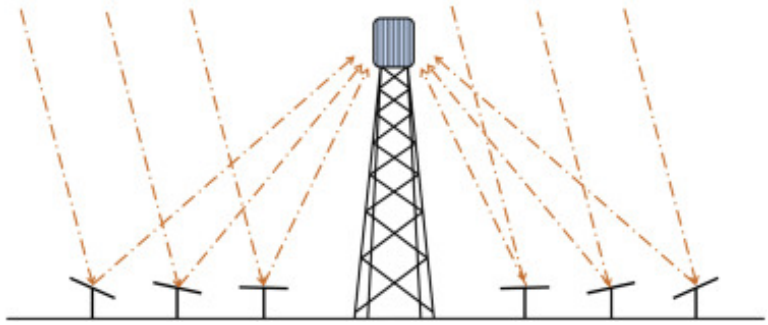

Figure 2.6: Solar central tower (Orosz and Dickes, 2017).

2.4 Thermal Storage

As the availability of solar power is limited throughout the day, thermal energy storage (TES) technologies are used to control when the energy absorbed by the sun is to be used for power generation. This allows for flexibility in the system, with the TES acting as a buffer between the solar collector and the power generating unit. The periods with the largest solar intensity does, for example, not correspond to the periods with the highest power demand. Thus, the energy can be stored in periods with high solar intensity and low power demand, and be used in periods with low solar intensity and high power demand (Pelay et al., 2017). Another application is to even out the variations in solar intensity and secure stable operation of the power generating unit through the whole day (Yang et al., 2019).

There are mainly three techniques for TES; sensible, latent, and thermochemical. About 50 % of existing CSP plants utilize TES. Among these, and in planned plants, sensible heat storage is by far the most used technology due to its maturity (Pelay et al., 2017).

2.4.1 Sensible Heat Storage

In sensible heat storage (SHS), the heat is stored by raising the temperature of a medium without undergoing a change in phase. Thus, the stored energy is dependent on the stored mass of the medium, the heat capacity of the medium, and the temperature difference before and after the charging of the storage (Orosz and Dickes, 2017).

2.4.1.1 Two-Tank Storage

Two-tank storage is often implemented for sensible TES. In these systems, one tank acts as a cold reservoir, while the other as a hot reservoir. The storage medium has to be a liquid as it needs to flow between the two tanks. We differentiate between direct and indirect storage for two-tank systems. In direct systems, the HTF used in the solar collector is also used as a storage medium in the tanks. Whereas for the indirect systems, the HTF and the

storage medium interact through a heat exchanger. This is illustrated in Figure 2.7 (Orosz and Dickes, 2017).

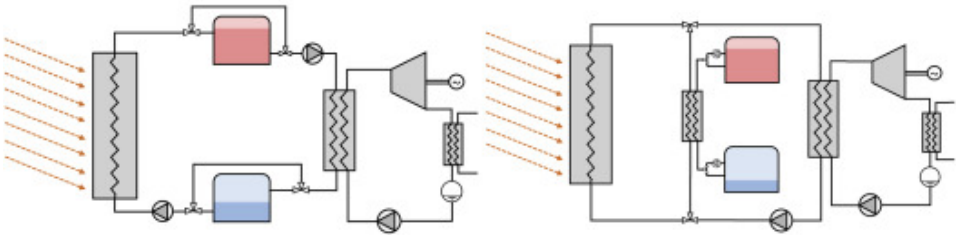

Figure 2.7: Direct (left) and indirect (right) TES (Orosz and Dickes, 2017).

Usually, molten salts or synthetic oils are used for these systems, as they are suited for high-temperature storage (Kuravi et al., 2013). In indirect systems, inorganic nitrate salt mixtures are preferred because they offer a good combination of density, specific heat, chemical reactivity, vapour pressure, and cost. A density of 1880 kg/m^3 and specific heat of 1500 J/kgK makes it suitable for storage. Low reactivity gives a stable system. Low vapour pressure allows for large vertical tanks to operate at atmospheric pressure. Low cost is desirable (in the range 0.40-0.90 US dollar per kg)(Herrmann et al., 2004).

2.4.1.2 Thermocline Storage

Thermocline storage systems can be considered a cheaper alternative to two-tank storage. In thermocline storage, the hot and cold storage medium is kept in the same tank. A thermal stratification between the hot and cold medium is maintained stable by buoyancy forces (Yang and Garimella, 2010). This creates a thermal gradient in the tank when the hot medium enters the top of the tank, displacing cold medium at the bottom of the tank (Kuravi et al., 2013). To further decrease the costs of the storage, it is common to use a solid filler material in the tank, displacing the more expensive molten salt or other media of choice. Examples of filler materials are quartzite rock and silica sand (Brosseau et al., 2004).

2.4.2 Latent Heat Storage

Latent Heat Storage (LHS) takes advantage of endothermic and exothermic nature of materials undergoing phase change for charging and discharging of the storage, respectively. Compared to SHS, LHS has a higher energy density per unit mass and unit volume (Sharma and Sagara, 2005). The phase change materials (PCMs) that can be used for latent storage are mainly organic materials (a range of acids, paraffin wax, urea and more) and salt hydrates. A problem with PCMs is their low thermal conductivities in combination with low rates of thermal diffusion, causing challenges regarding the charge and discharge rates of the storage (Da Cunha and Eames, 2016).

2.4.3 Thermochemical Heat storage

Thermochemical heat storage (THS) has the highest energy density potential of storage technologies. However, the technology is still at a research and development stage and not in commercial use (H Abedin and A Rosen, 2011). THS relies on reversible chemical reactions to store energy. Heat is stored by applying it to drive an endothermic reaction, and released by the reverse, exothermic, reaction (Orosz and Dickes, 2017). The general concept of charging, storing, and discharging for a THS is shown in Figure 2.8.

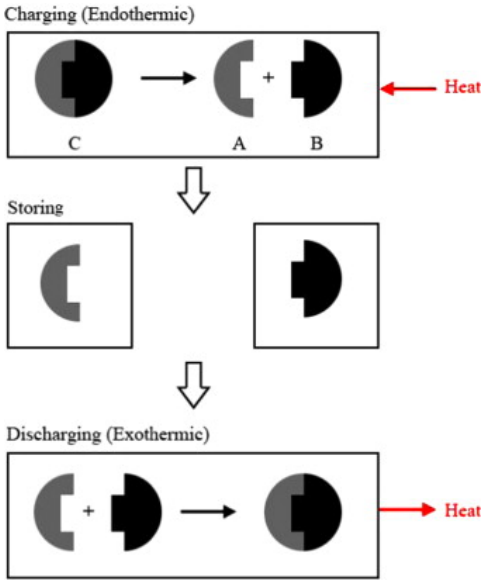

Figure 2.8: Charging, storing and discharging for THS (Mahlia et al., 2014).

2.5 Organic Rankine Cycle

The organic Rankine cycle (ORC) is a prominent technology for low to medium heat-to-power generation (up to 400 °C) (DiGenova et al., 2013). It has the same working principles as that of the conventional steam Rankine cycle, using organic working fluids instead of water. Although there are other technologies capable of operating in the same temperature range, such as the Kalina cycle and the Goswami cycle, the ORC offers several advantages. For low to medium temperature heat sources, the thermal efficiency is acceptable compared to other technologies (Chen et al., 2010). The basic layout of the ORC is very simple, consisting only of a pump, an evaporator, a turbine, and a condenser. However, more advanced layouts are possible and are often used. Nevertheless, even the most basic layout can offer relatively high efficiency. In combination with advantageous properties of the organic working fluid, such as low mechanical stress in the turbine (Macchi and Astolfi, 2016), the ORC offers reliable and relatively simple energy conversion with thermal efficiency at a competitive level.

2.5.1 Working Principle

The most basic ORC layout consists of a pump, an evaporator, a turbine, and a condenser. Through four different processes, the organic working fluid is circulating through the different components. First, the working fluid is pumped to evaporation pressure from condensation pressure. Second, the working fluid is evaporated in the evaporator, absorbing heat. Third, the working fluid is expanded through the turbine, generating work. Fourth and last, the working fluid is condensed, flowing through the condenser. The thermal efficiency for the ORC is defined as the ratio of power to heat absorbed in the evaporator. A simple ORC layout and corresponding T-S diagram are shown in Figure 2.9.

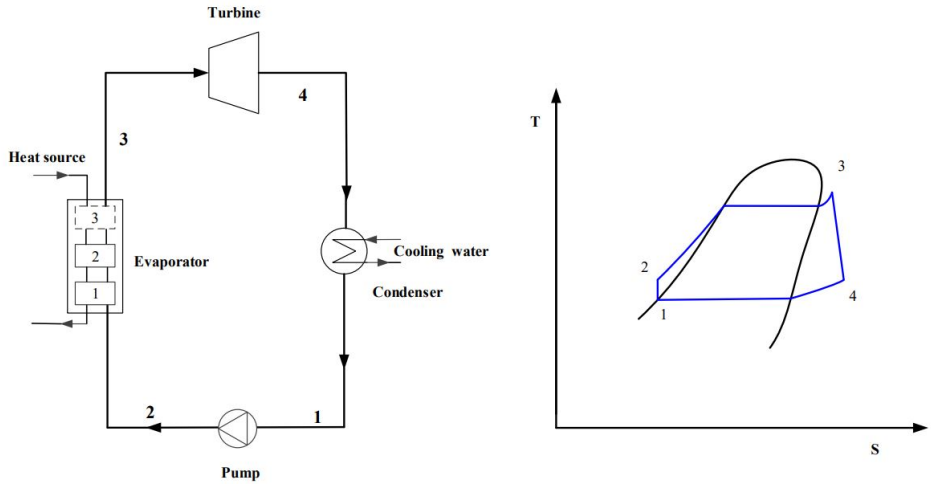

Figure 2.9: Basic ORC layout and T-S diagram (Yu, 2016).

There are a number of different possibilities regarding modifications to the basic ORC. As it stands in its most basic form, any remaining heat after the expansion process in the turbine goes to waste in the condenser. By connecting a heat exchanger or recuperator between states 2 and 4 in Figure 2.9, the remaining heat can be used to preheat the working fluid before it enters the evaporator. Thus, less heat goes to waste, and the thermal efficiency increases (Yu, 2016). This is called a recuperative ORC, and the layout and corresponding T-S diagram can be seen in Figure 2.10. As it only adds one additional component to the cycle, it is a relatively simple and common modification to the ORC.

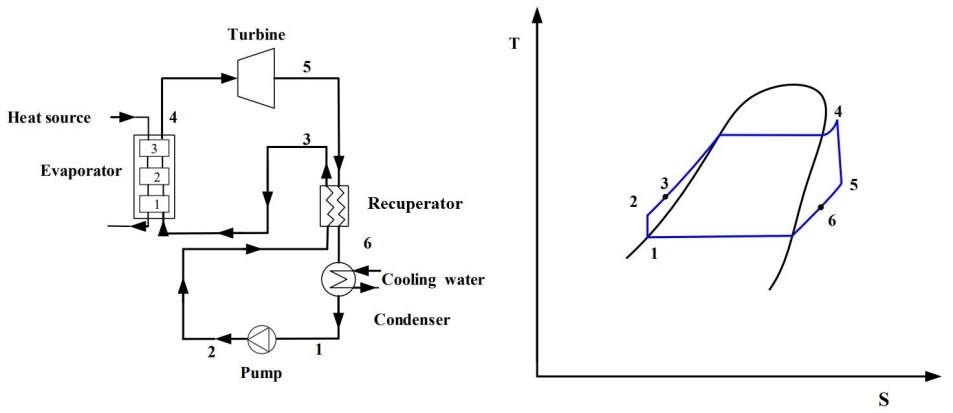

Figure 2.10: Recuperative ORC with T-S diagram (Yu, 2016).

Another modification is to incorporate turbine bleeding. This is done by removing a portion of the working fluid from the turbine and mixing it with the working fluid at a lower pressure and temperature. Turbine bleeding can also be combined with a regenerator, as shown in Figure 2.11.The turbine bleeding increases the thermal efficiency by increasing the working fluid temperature at the inlet of the evaporator (Yu, 2016).

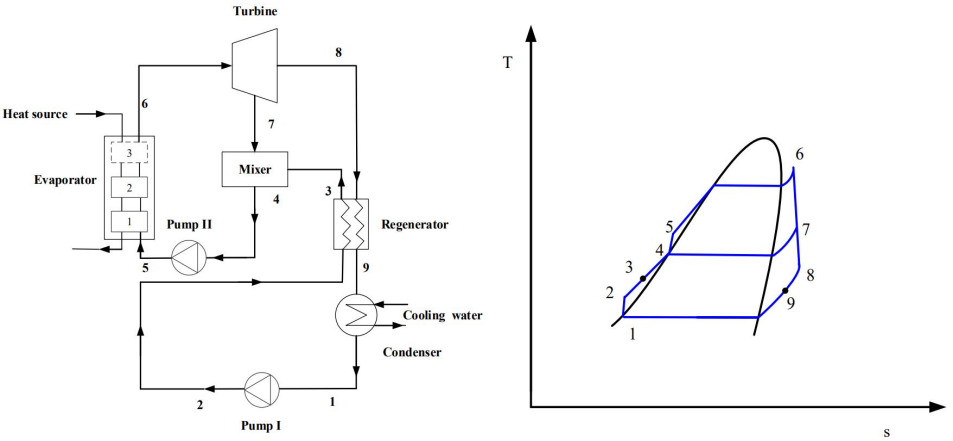

Figure 2.11: Regenerative ORC with turbine bleeding and corresponding T-S diagram (Yu, 2016).

Safarian and Aramoun (2015) performed an energy and exergy assessment of modified ORCs. The basic ORC was assessed, along with a regenerative modification, a turbine bleed modification, and an ORC incorporating both turbine bleeding and a regenerator. The results showed that the thermal efficiencies were 19.46 %, 21.5%, 22%, and 22.83%, respectively, for the same evaporator duty and working fluid. For the latter three, the exergy losses in the evaporator decreased by 5.5%, 48.5%, and 55%, respectively, compared to the basic ORC. All the modifications raise the temperature of the working fluid at the

evaporator inlet, increasing the thermal and exergetic efficiencies. In addition to raising the evaporator inlet temperature, the modifications decrease the cold utility demand in the condenser, further increasing the total exergetic efficiency of the cycle.

2.5.2 Organic Working Fluid

The selection of the right organic working fluid is essential for the ORC. The fluid can be either a pure (single) component organic fluid, or a multicomponent fluid. The pure fluids can be classified as either wet, dry or isentropic fluids, depending on the slope of their vapour saturation curve seen in the T-S diagram (Chen et al., 2010). Wet fluids have a positive curve, dry fluids have a negative curve, and isentropic fluids have a near vertical (infinite or isentropic) curve. Multicomponent fluids are mixtures of different organic fluids, giving the mixture gliding condensation and evaporation temperatures, instead of constant, as for the pure fluids. This makes multicomponent fluids favorable when, for example, condensing the fluid with heat from non-isothermal heat sources (Lee and Mitsos, 2017).

An important feature of the dry and isentropic organic working fluids is that they eliminate the need for superheating before the expansion in the turbine. Wet fluids, on the other hand, need some degree of superheating to avoid condensation at the turbine outlet. This is illustrated in Figure 2.12 where a wet and a dry organic working fluid is shown.

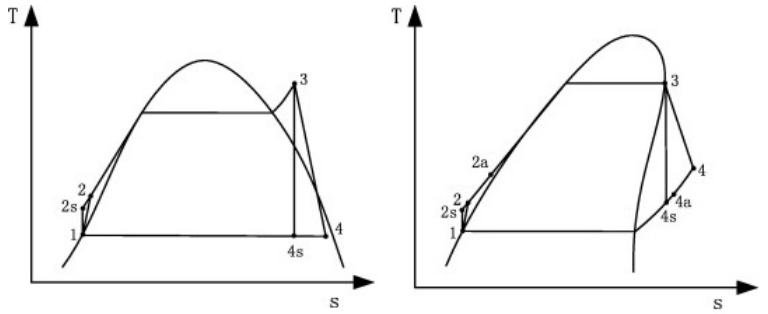

Figure 2.12: T-S diagrams of wet (left) and dry (right) organic working fluids (Dai et al., 2009).

2.5.2.1 Organic Working Fluid Selection

For small to medium scale plant, the dry working fluids have proven to be the most efficient. The dry fluid allows the turbine to operate at nearly the same efficiencies regardless of the fluid is saturated vapour or superheated vapour. Also, problems such as blade erosion are eliminated due to no condensation in the expansion process in the turbine(Desai and Bandyopadhyay, 2016). For SORCs, utilizing energy source temperatures up to 400°C, toluene has been found to be the most efficient organic working fluid (Desai and Bandyopadhyay, 2016; Yang et al., 2019; Mavrou et al., 2015). This makes toluene a suitable choice when using concentrating solar collectors with high concentration ratios.

Aboelwafa et al. (2018) performed a review and classified a series of pure working fluids used in investigations of SORCs. Some of the common fluids and their appropriate turbine inlet temperatures are listed in Table 2.1.

Working fluid	**Classification**	**Turbine inlet temperature**
Propane (R290)	HC	68.2-120°C
Butane (R600)	HC	70-170°C
Isobutane (R600a)	HC	80-150°C
Pentane (R601)	HC	70-213.7°C
Isopentane (R601a)	HC	80-289°C
Cylohexane	HC	75-302°C
Benzene	HC	100-294°C
Toluene	HC	280-380°C
Ethylbenzene	HC	342°C
Ethanol	Alcohol	75-150°C
R134a	HFC	50-200°C
R245fa	HFC	70-250°C
R123	HCFC	75-200°C
MM (octamethyltrisiloxane)	Siloxane	235-400°C

Table 2.1: Working fluids, their classification and typical turbine inlet temperatures. (Classifications: HC: Hydrocarbon, HFC: Hydrofluorcarbon) (Aboelwafa et al., 2018)

When selecting the working fluid, a number of considerations have to be taken into account. Thermodynamic and physical properties have a direct impact on the ORC performance in a number of ways:

- Higher vapour density gives a lower volumetric flow rate, which results in smaller equipment (McMahan, 2006).
- Low viscosity increases the heat transfer coefficient (Quoilin, 2011).
- Thermal conductivity affects the heat transfer in heat exchangers (Aboelwafa et al., 2018).
- For single-stage turbines, the molecular weight of the fluid should be above 90 g/mol (Tchanche et al., 2009).
- The liquid specific heat capacity should be low for higher work output(Chen et al., 2010).
- The condensation pressure of the fluid should ideally be equal to or higher than the atmospheric pressure to avoid vacuum or leakage (Aboelwafa et al., 2018).
- The fluid must have a lower freezing point than the lowest temperature of the cycle (Quoilin, 2011).

- The thermal stability of the fluid must be considered, and be within the operating range of the cycle (Chen et al., 2010).

Other aspects that should be considered are:

- Environmental impacts, such as global warming potential (GWP) and ozone-depleting potential (ODP), should be considered (Schuster et al., 2007).
- Safety aspects due to dangers related to toxicity, flammability, and danger of explosions (Schuster et al., 2007).
- Compatibility between the fluid and materials in the cycle (Aboelwafa et al., 2018).
- Economy. The fluid itself can be expensive, while compatibility and safety aspects can affect the cost (Aboelwafa et al., 2018).

The effect of the working fluid selection has been the subject of many investigations regarding ORC performance. Some of the findings and conclusions are presented as follows:

- When there are no constraints to the target temperature of a sensible heat source, the optimal working fluid should have a critical temperature 25-35°C below the heat source temperature (Yu et al., 2016).
- Fluids with higher critical temperature gives better ORC performance (Rayegan and Tao, 2011; Bruno et al., 2008).
- Heavier fluids generally achieve higher turbine efficiencies (Harinck et al., 2009).

2.6 Heat Transfer Fluid

The heat transfer fluid (HTF) is essential for SORCs with thermal storage. Although it causes irreversibilities in heat exchangers, that could be avoided by using direct evaporation of the ORC working fluid in the solar collector, these losses can not be avoided when incorporating thermal storage (Aboelwafa et al., 2018).

The heat transfer fluid (HTF) is essential for SORCs with thermal storage. Irreversibilities in heat exchangers can be avoided by using direct evaporation of the ORC working fluid in the solar collector. These losses can, however, not be avoided when incorporating thermal storage (Aboelwafa et al., 2018).

As for the organic working fluid selection for the ORC, the choice of the HTF must be made with considerations to the operating conditions of the system of where it is to be applied.

Chapter 3

Modelling

This chapter presents the tools, algorithms, assumptions, and models for simulating a solar organic Rankine cycle (ORC) with thermal storage, operating with stable power output. The ORC is modelled using the software Aspen HYSYS V9, while the thermal storage and solar collector are modelled in Matlab R2018b. The optimal operating points for the ORC are found by running a particle swarm optimization (PSO) algorithm in Matlab. The connection between Matlab and HYSYS makes up a simulation-based optimization framework based on the proposed model.

3.1 Aspen HYSYS

HYSYS has been used to simulate and the organic Rankine cycle, and through interaction with Matlab, to optimize the process. An important feature is that it allows the user to select the equations of state, depending on the application of the program. In this thesis, the Peng-Robinson equation of state has been used.

The software is an engineering simulation tool developed by AspenTech, a company founded at the chemical engineering group at MIT in 1981. It was the result of a grant given by the U.S. Department of Energy, encouraging innovation in the process industries following the oil crisis in the 1970s (AspenTech, 2019). HYSYS is a powerful tool, designed with the purpose of interactive operation. A wide range of processes can be simulated through both dynamic and steady-state operation, rooted in a strong thermodynamic foundation (Hamid, 2007) .

3.1.1 Peng-Robinson Equation of state

The Peng-Robinson (PR) equation of state (EOS) was presented in 1976 to give more reliable predictions of thermodynamic properties than the commonly used equations at the time (Peng and Robinson, 1976). The PR EOS is defined with the critical properties and the acentric factor and yields good accuracy near the critical point when calculating

compressibility and liquid density (Nasri and Binous, 2009). It is the most enhanced model in Aspen HYSYS, offering the largest range in terms of temperature and pressure, and is regarded particularly suitable for systems with hydrocarbons (Sunny et al., 2016).

3.2 Matlab

Matlab has been used to implement equations, in order to model a simple parabolic trough solar collector and a two-tank direct storage system. It has also been used to write small programs to be implemented in the final model. The most powerful implementation, however, is running the particle swarm optimization algorithm, providing the optimal results for the simulations.

The software was first available as a commercial program in the early 1980s. MathWorks, founded by some of Matlabs original developers, was founded in 1984 and has been offering the software ever since. The program is based on matrix computations, which makes it well suited for numerical analysis and numerical calculations (Moler, 2004).

3.2.1 Particle Swarm Optimization

Kennedy and Eberhart developed the Particle Swarm Optimization (PSO) algorithm in 1995, inspired by the behaviour of bird flocking and their ability to localize food as a group. The algorithm describes a population containing particles, representing possible solutions. Each individual particle has its own position and velocity vector, and a fitness value describing the quality of its position. This gives each particle an internal state, which is visible to the whole population. The direction and speed at which the individual particles move across the search space are influenced by their own best position found so far, the local best position found by neighbouring particles, and the best global position found so far. As the algorithm iterates, the particles will converge to the optimal position, or solution (Kennedy and Eberhart, 1995; Liu et al., 2017).

The PSO is visualized in Figure 3.1. It illustrates the convergence towards local optima before all the particles converge to the global optimum.

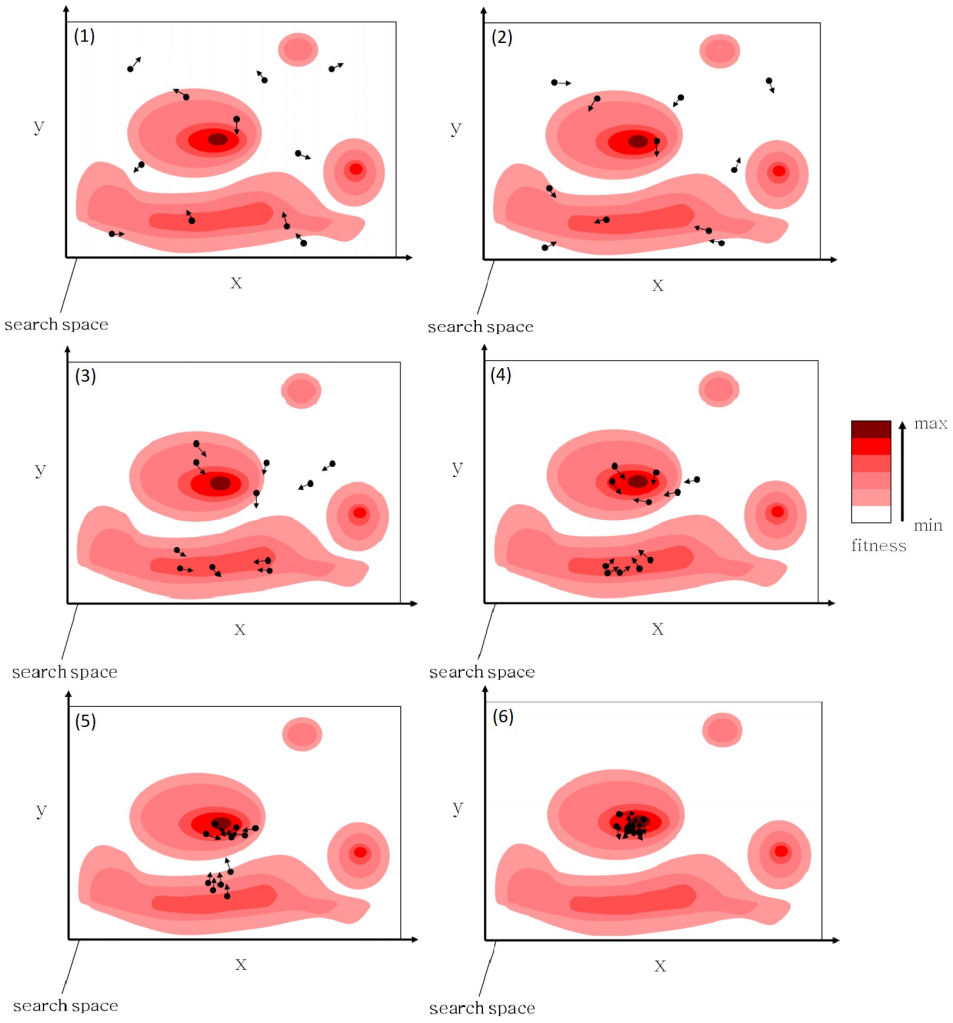

Figure 3.1: Visualization of swarm progression from 1 to 6 (Kennedy and Eberhart, 1995).

3.3 Model Description

The model developed for this project represents a solar-powered organic Rankine cycle power plant with thermal storage. The system is modelled with two different configurations for the ORC, a basic cycle and a recuperative cycle. The parabolic trough collector (PTC) was selected as the solar collector as it is able to heat the heat transfer fluid (HTF) to relatively high temperatures, it has good efficiency, and it is, in general, a well-proven technology. The storage unit selected is a two-tank direct system. This simplifies the model since only few heat exchangers are required. The fact that the two-tank system is

common and well-proven technology is also an important decision factor. The schematic of the system is shown in Figure 3.2.

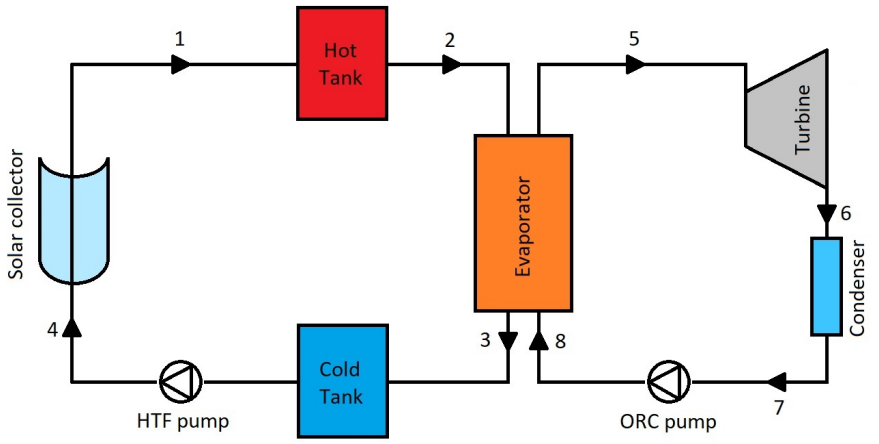

Figure 3.2: Schematic of the proposed system model with a basic ORC layout.

As Figure 3.2 shows, the system consists of two cycles connected by a counter-current heat exchanger. The solar cycle (points 1-2-3-4) circulates a thermal oil as HTF, receiving heat from the solar collector, before entering the hot storage tank. The HTF delivers heat to the ORC between points 2 and 3 before entering the cold storage tank. The purpose of the storage tanks is to add a buffer that converts the variable energy from the sun into constant energy delivered to the evaporator of the ORC. This is achieved by controlling the HTF pump, adjusting the mass flow rate through the solar collector so that it delivers HTF at a constant temperature to the hot tank. This includes reducing the mass flow rate to zero when there is not sufficient solar radiation to reach the constant temperature. The HTF is then released at a constant mass flow rate to the evaporator, where it delivers heat and is cooled. Because the ORC (points 5-6-7-8) operates at steady conditions, with a constant heat consumption in the evaporator, the HTF is also delivered to the cold tank at a constant temperature. The ORC circulates an organic working fluid, evaporated by the HTF between points 8 and 5. The working fluid enters the turbine, where it is expanded before entering the condenser. The working fluid is condensed by means of external cooling water. The fully condensed fluid is then pumped to evaporation pressure before reentering the evaporator.

The system incorporating the recuperative ORC was developed by keeping the solar cycle from Figure 3.2 and fitting the ORC with a recuperator. This allows for higher efficiencies with rather small changes to the system layout. The system layout of the recuperative model is done, as shown in Figure 3.3.

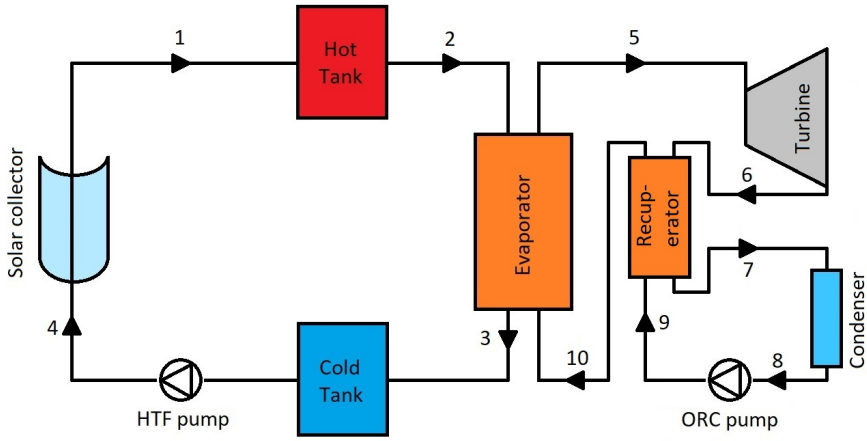

Figure 3.3: Schematic of the proposed system model with recuperative ORC layout.

This modification makes up a recuperative ORC and adds more points to the cycle. The main difference with respect to the basic ORC is that some of the heat exiting the turbine in point 6 is used to preheat the working fluid (process between points 9 and 10) before entering the evaporator. In addition to reducing the cooling requirement in the condenser, this will also increase the temperature of the working fluid entering the evaporator in point 10. This lowers the temperature difference of the working fluid at points 10 and 5 and also the temperature difference of the HTF at points 2 and 3. As a consequence, this will have an effect on the mass flow rates in both the solar cycle and the ORC compared to the basic layout in Figure 3.2.

3.4 Methodology

This section describes the modelling of the different parts that make up the complete model, as well as assumptions made. The solar cycle part is modelled using Matlab, whereas the ORC part is modelled using HYSYS.

3.4.1 Solar Data and Site Data

The solar irradiation data and ambient temperatures used for calculation purposes are very similar to those presented by Yang et al. (2019), which represent a summer day in the northwest of China. These data were chosen so that the model can be compared with other models and results, using similar data.

The data represents only one day, which is divided into 24 time steps. The irradiation and ambient temperatures are assumed to be constant for each time step. For each time step the available energy from the sun, Q_s, can be calculated by Equation 3.1:

$$Q_s = ac \cdot G_b \tag{3.1}$$

where ac is the aperture area of the collector, and G_b is the solar beam irradiation, or the direct normal irradiation (DNI). The data for DNI and the ambient temperatures are given in Figure 3.4 and Figure 3.5, respectively.

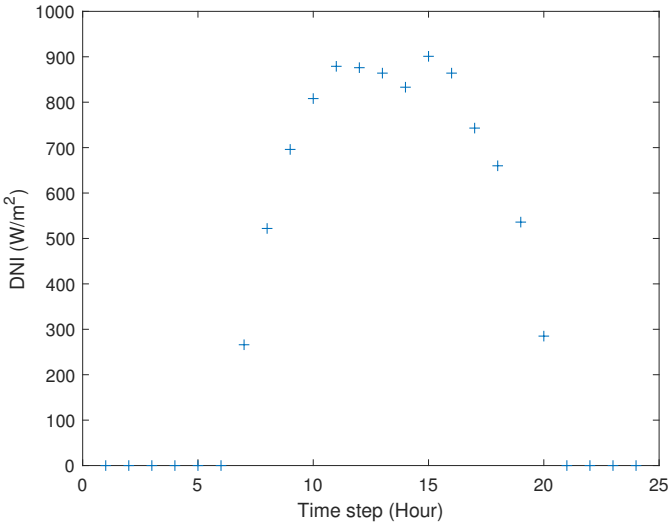

Figure 3.4: DNI for a given summer day.

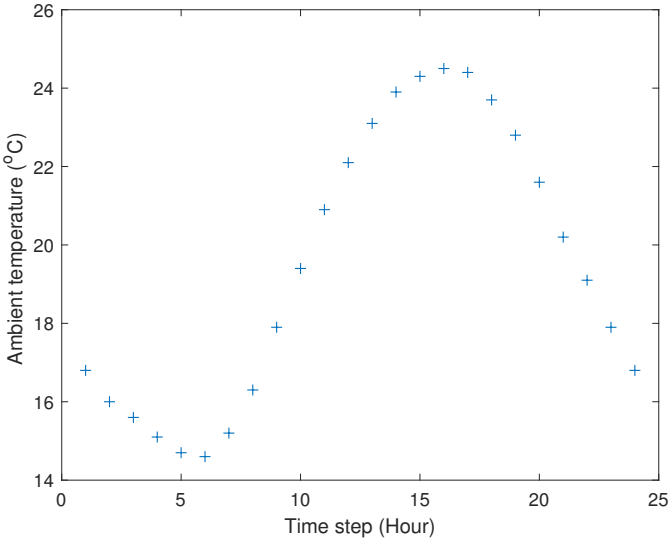

Figure 3.5: Ambient temperatures for a given summer day.

3.4.2 Solar Collector

The PTC chosen for modelling purposes is the commercially available EuroTrough ET-150. This model was found to be both economical and effective for similar system layouts by Tzivanidis et al. (2016). The efficiency of the collector is given by Equation 3.2, as suggested by Blanco et al. (2003).

$$\eta_c = 0.75 - 0.000045\Delta T - 0.039\frac{\Delta T}{G_b} - 0.0003G_b(\frac{\Delta T}{G_b})^2 \tag{3.2}$$

where ΔT is the difference between ambient and mean temperatures in the collector, and G_b is the beam irradiation.

Given the temperatures of the HTF at the inlet, T_2, and outlet, T_3, the required mass flow through the collector, $\dot{m}_c$, can be found using the relation in Equation 3.3:

$$\dot{Q}_c = \dot{m}_c \cdot c_{p,HTF} \cdot (T_2 - T_3) \tag{3.3}$$

where $\dot{Q}_c$ is the energy the HTF can absorb in the collector. The relationship between $\dot{Q}_c$ and the available energy from the sun, $\dot{Q}_s$, is given by Equation 3.4:

$$\eta_c = \frac{\dot{Q}_c}{\dot{Q}_s} \tag{3.4}$$

The only losses related to the solar collector are the ones induced by the efficiency of the solar collector.

3.4.3 Thermal Storage

The thermal storage is modelled as a direct two-tank system, where the HTF can accumulate in the tanks. The tanks are assumed without losses, meaning that the temperature of the HTF entering, stored and leaving the hot tank is constant at temperature T_{hot} and constant at temperature T_{cold} for the cold tank. In addition, the tanks are assumed to have the capacity to store enough HTF for one day of operation, and enough initial storage to supply the ORC before there is available energy from the sun.

The constant mass flow rate of the HTF delivered from the hot tank is calculated by first calculating how much HTF that would accumulate in the hot tank throughout the whole day, without any supply to the evaporator. The constant mass flow rate is then the rate which would empty the tank in one day if there where no HTF entering the hot tank.

As the HTF circulates between the hot and the cold tanks, there are two different mass flow rates in the solar cycle. The constant flow leaving the hot tank, passing through the evaporator and entering the cold tank, $\dot{m}_{HTF}$, and the variable flow through the solar collector from the cold tank to the hot tank, $\dot{m}_c$. The work done by the pump circulating the HTF is assumed to be negligible.

3.4.4 Evaporator

The evaporator is modelled as a counter-current heat exchanger without losses. The equation governing its energy balance is thereby given by Equation 3.5:

$$\dot{Q}_{evap} = \dot{m}_{HTF} \cdot c_{p,HTF} \cdot (T_2 - T_3) = \dot{m}_{ORC} \cdot (h_5 - h_{8(10)}) \tag{3.5}$$

where h is the specific enthalpy of the ORC working fluid before the evaporator. The point in parenthesis indicates the point used for the recuperative ORC in Figure 3.3. This notation is used throughout this chapter.

The only limiting factor in the evaporator is the minimum approach temperature, or the pinch point temperature. This is set at a minimum of 10°C, but can be adjusted to a higher temperature for the purpose of comparison with other models.

3.4.5 Heat Transfer Fluid

Synthetic organic thermal oils are commonly used as HTF in parabolic trough collectors. The thermal oil is a mixture of Diphenyl oxide and Biphenyl, where a mass mixture ratio of 73.5% and 26.5%, respectively, can be used for temperatures up to 400°C before becoming unstable (Lang and Lee, 2015). Because of this limitation to the thermal oil, the HTF temperature of the system should not exceed 400°C.

To calculate the mass flow rate of the HTF in the solar cycle, the specific heat capacity of the mixture, $c_{p,HTF}$, needs to be known or estimated. Due to difficulties in acquiring accurate values for this particulate mixture, the specific heat capacity is estimated through regression, using data available in Aspen HYSYS. Figure 3.6 shows the data from HYSYS and the estimated specific heat capacity as a function of temperature.

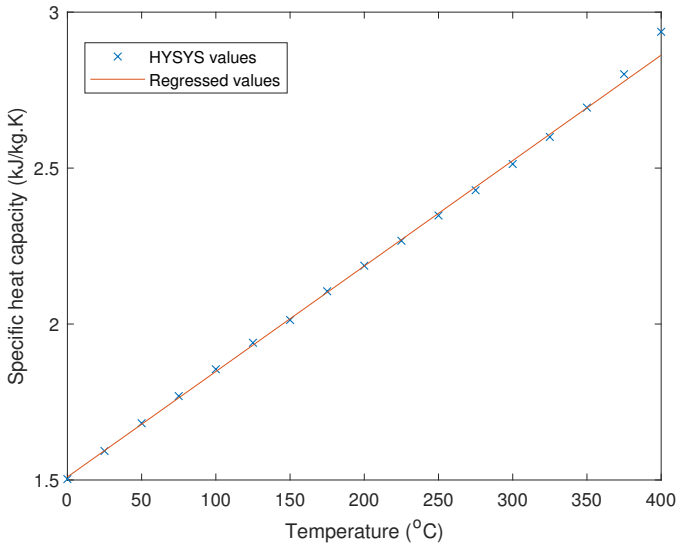

Figure 3.6: The estimated (regressed) values of the specific heat capacity as a function of temperature compared with values from HYSYS.

The value of the specific heat capacity as a function of temperature can be expressed as follows:

$$c_{p,HTF} = 3.3811T + 1509.7 \tag{3.6}$$

where T is the temperature in °C and the unit of $c_{p,HTF}$ is given as J kg^{-1} K^{-1}. Figure 3.6 shows that Equation 3.6 becomes inaccurate at temperatures from 375°C to 400°C, thus decreasing the accuracy of the model at the highest temperature levels. The maximum temperature should, therefore, be limited to 375°C.

3.4.6 Organic Rankine Cycle

The power developed by the turbine can be expressed as follows:

$$\dot{W} = \dot{m}_{ORC} \cdot (h_5 - h_6) \tag{3.7}$$

The isentropic efficiency of the turbine is given as:

$$\eta_{turbine} = \frac{h_5 - h_6}{h_5 - h_{6,s}} \tag{3.8}$$

where $h_{6,s}$ is the enthalpy of the working fluid at the turbine outlet in the case of an isentropic expansion.

For the recuperating ORC, the recuperator is modelled as an counter-current heat exchanger, and the calculations related to it is identical to that of the evaporator previously described. Thus, the duty of the recuperator and the relationship between the hot and cold side is as follows:

$$\dot{Q}_{rec} = \dot{m}_{ORC} \cdot (h_6 - h_7) = \dot{m}_{ORC} \cdot (h_{10} - h_9) \tag{3.9}$$

The condenser is modelled as a cooler. The duty is expressed as follows:

$$\dot{Q}_{cool} = \dot{m}_{ORC} \cdot (h_{6(7)} - h_{7(8)}) \tag{3.10}$$

By regarding the condenser as a heat exchanger, similar to the evaporator and the recuperator, and using water for cooling, the required work for pumping water is expressed as:

$$\dot{W}_{pump,cool} = \frac{\dot{Q}_{cool}}{(h_{water,out} - h_{water,in})} \cdot g \cdot H \tag{3.11}$$

where g is the gravitational acceleration, and H is the cooling pump pressure head. Assuming that the cooling water is supplied at 20°C and is heated to 30°C, $h_{water,in}$ and $h_{water,out}$ represents the specific enthalpies of water at these temperatures, respectively.

The required work to drive ORC pump is given by the following expression:

$$\dot{W}_{pump,ORC} = \dot{m}_{ORC} \cdot (h_{8(9)} - h_{7(8)}) \tag{3.12}$$

The isentropic efficiency of the pump is expressed as follows:

$$\eta_{pump,ORC} = \frac{h_{8(9),s} - h_{7(8)}}{h_{8(9)} - h_{7(8)}} \tag{3.13}$$

where $h_{out,s}$ is the enthalpy of the working fluid at the outlet for isentropic compression.

3.4.7 System Efficiencies

For systems producing electricity, the efficiency of motors driving pumps and generators driven by the turbine must be included to calculate the system efficiencies.

The electricity generated by the turbine is defined as follows:

$$\dot{P}_{turbine,el} = \eta_{generator} \cdot \dot{W} \tag{3.14}$$

where $\eta_{generator}$ is the efficiency of the electric generator, and $\dot{W}$ is the power generated by the turbine.

The power required to drive the ORC pump is expressed by Equation 3.15.

$$\dot{P}_{pump,el} = \frac{\dot{W}_{pump}}{\eta_{motor}} \tag{3.15}$$

where $\dot{W}_{pump}$ is the work required by the pump (ORC pump or cooling water pump) and η_{motor} is the efficiency of the motor driving the pump.

The efficiency of the ORC is given by Equation 3.16.

$$\eta_{ORC} = \frac{\dot{W}_{net}}{\dot{Q}_{evap}} \tag{3.16}$$

where $\dot{W}_{net}$, the net power output, is given by Equation 3.17:

$$\dot{W}_{net} = \dot{P}_{turbine,el} - \dot{P}_{pump,el,ORC} - \dot{P}_{pump,el,cool} \tag{3.17}$$

and $\dot{Q}_{evap}$ is the heat delivered to the evaporator of the ORC.

The efficiency of the solar cycle is given by the following expression:

$$\eta_{solar} = \frac{\dot{Q}_{evap}}{\Sigma\dot{Q}_s/n_{ts} \cdot ac} \tag{3.18}$$

where $\Sigma\dot{Q}_s$ is the sum of the available energy from the sun at each time step, n_{ts} is the number of time steps, and ac is the aperture area.

Finally, the total system efficiency is given by Equation 3.19.

$$\eta_{system} = \eta_{ORC} \cdot \eta_{solar} \tag{3.19}$$

3.4.8 Parameters and Variables

The model contains a number of design parameters, input parameters and optimization variables. Some of the design parameters are taken from a similar design (Yang et al., 2019), those are shown in Table 3.1.

Design parameter	Value
Turbine isentropic efficiency ($\eta_{turbine}$)	0.80
ORC pump isentropic efficiency ($\eta_{pump,ORC}$)	0.75
Motor efficiency (η_{motor})	0.75
Gravitational acceleration (g)	9.81 m/s^2
Cooling pump pressure head (H)	10 m

Table 3.1: Design parameters.

Input parameters are shown in Table 3.2. These parameters can be changed to fit the case that is to be optimized by the model.

Input parameter	Symbol
Minimum approach temperature, heat exchangers	ΔT_{min}
Condensation temperature ORC	T_{cond}
Aperture area	ac
Solar beam radiation	G_b
Ambient temperature	Tam

Table 3.2: Input parameters.

The variables that are optimized by the model for the basic ORC are shown in Table 3.3. For the recuperative ORC, the model also optimizes the duty of the recuperator, as shown in Table 3.4

Optimization variable	Symbol
Hot tank temperature	T_{hot}
Cold tank temperature	T_{cold}
Molar flow rate ORC	$\dot{n}_{ORC}$
ORC evaporation pressure	p_{evap}

Table 3.3: Optimization variables for the basic ORC.

Optimization variable	Symbol
Hot tank temperature	T_{hot}
Cold tank temperature	T_{cold}
Molar flow rate ORC	$\dot{n}_{ORC}$
ORC evaporation pressure	p_{evap}
Recuperator duty	$\dot{Q}_{rec}$

Table 3.4: Optimization variables for the recuperatirve ORC.

Note that the hot and cold tank temperatures are the same temperatures as the temperatures of the HTF at the inlet and outlet of the evaporator, T_2 and T_3, respectively.

With values for all the before mentioned parameters, all other parameters related to the system are either found by the relations given in this chapter, or can be found in the ORC model in HYSYS.

3.4.9 Optimization

HYSYS and Matlab allow for interaction between the two programs. When running the particle swarm optimization (PSO) algorithm in Matlab, the program reads parameters and variables from HYSYS, processes the data, and writes new values for the variables in the HYSYS model. The PSO algorithm will run iterations until the change in the objective function becomes negligibly small. The objective function for the model is maximum net power output from the ORC. For each iteration, values for the optimization variables are guessed based on previous iterations and within set boundaries and constraints. The boundaries are set based on technical and practical limitations of the HTF and the organic working fluid. The constraints ensure that the vapour fraction at the turbine inlet is 1 and that the approach temperatures in the heat exchangers are above their minimum value. One iteration can, in short, be summarized as follows:

1. The optimization values are given values
2. $\dot{m}_{HTF}$ is calculated based on T_{hot}, T_{cold}
3. $\dot{Q}_{evap}$ is calculated based on $\dot{m}_{HTF}$, T_{hot} and T_{cold}
4. $\dot{W}$ is calculated based on $\dot{Q}_{evap}$, $\dot{m}_{ORC}$ and p_{evap}
5. The result is checked against the constraints and kept if it is better than previous iterations

Chapter 4

Results and Discussion

This chapter evaluates the performance of the model and the simulation-based optimization. The results are discussed continuously as they are presented.

4.1 Performance of the ORC

To evaluate the performance of the model, it is compared to a model by Yang et al. (2019). Based on the sources stated in the paper, it appears to have used incorrect equations for the efficiency of the solar collector, making comparisons of the total system uninteresting. The performances of the ORCs, however, are comparable. Toluene was used as the organic working fluid, which was also used by the reference model.

4.1.1 Basic ORC

Parameter/variable	Reference Model	Proposed model
T_{hot}	375°C	375°C
T_{cold}	71.7°C	71.7°C
p_{evap}	37.12 bar	37.12 bar
$T_{inlet,turbine}$	311.5°C	311.5°C
η_{ORC}	22.2%	22.5%

Table 4.1: Comparison of the performance between the model given by Yang et al. (2019) and the model proposed in this project.

Table 4.1 shows that the efficiency achieved from the model used in this thesis is slightly higher than for the one proposed by Yang et al. (2019). This difference can, to some degree, be explained by the fact that the condenser is modelled differently in the two models. In addition, one of the variables that is optimized by the model, $\dot{n}_{ORC}$, is not

stated in Table 4.1. This is due to the parameter not being given by the reference. However, the temperature at the turbine inlet is given, $T_{inlet,turbine}$, which in combination with the other parameters, gives a set value for $\dot{n}_{ORC}$.

There is, however, a problem with this comparison. The values given in Table 4.1 gives a vapour fraction of 0 at the inlet of the turbine in the proposed model, which is infeasible by the constraints, and makes the result invalid. By restricting the vapour fraction to 1, i.e., saturated vapour, at the turbine inlet, the proposed model operation is feasible. The result of this is shown in Table 4.2.

Parameter/variable	Reference Model	Proposed model
T_{hot}	375°C	375°C
T_{cold}	71.7°C	71.7°
p_{evap}	37.12 bar	37.12 bar
$T_{inlet,turbine}$	311.5°C	313.3°C
η_{ORC}	22.2%	23.1%

Table 4.2: Comparison of the performance between the reference model and the proposed model using toluene as the organic working fluid.

As Table 4.2 shows, the proposed model requires a slightly higher temperature to reach saturated vapour at the turbine inlet compared to the reference model. The reason for this is that the working fluid becomes very sensitive to changes in temperature in the region where it transitions from saturated liquid to saturated vapour. This is illustrated by Figure 4.1

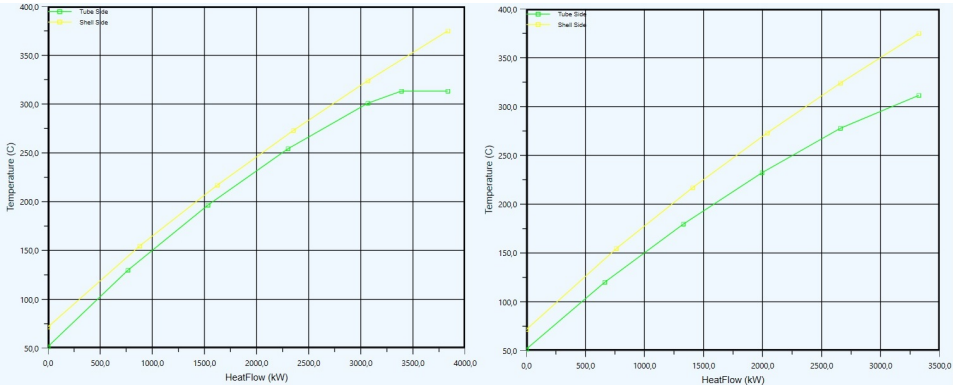

Figure 4.1: Heat curve of the working fluid (green line) in the evaporator. The working fluid is heated to 313.3°C (saturated vapour) (left) and to 311.5°C (right) along the same isobar. The yellow line is the heat curve of the HTF in the solar cycle.

At 311.5°C, the working fluid has not yet begun the evaporation process, while at 313.3°C the working fluid has become saturated vapour. Though the temperature difference is minimal, the required heat to fully evaporate the working fluid is significant. Thus,

the energy of the working fluid in the saturated vapour phase is significantly higher than for the working fluid in the saturated liquid phase.

4.1.2 Recuperative ORC

Parameter/variable	Reference Model	Model
T_{hot}	375°C	375°C
T_{cold}	251.9°C	251.9°C
p_{evap}	27.12 bar	27.12 bar
$\dot{n}_{ORC}$	207.1 kmol/s	207.1 kmol/s
$T_{inlet,turbine}$	355°C	355°C
η_{ORC}	30.4%	30.4%

Table 4.3: Comparison of the performance of the recuperative ORC for the reference model and the proposed model.

Table 4.3 shows that the under the same conditions, the recuperative ORC model performs at the same efficiency as the reference model. This indicates that the proposed model is fairly robust and reliable.

4.2 Optimization

For all the cases optimized, the same solar data, ambient temperature data, and collector aperture area were used. There are no losses associated with the aperture area. Changing the area will, therefore only alter the mass flows, power output, and the duties of the different heat exchangers. As these values are proportional to the aperture area, the efficiencies proved to be unaffected by changes to the aperture area. The aperture area used was therefore 1000 m^2 for all cases. Toluene was used as the organic working fluid if not otherwise stated.

4.2.1 Design Parameters from Reference Model

In this case, the system model is optimized using the design parameters from the reference model. The boundaries used for the optimization are shown in Table 4.4. The design and input parameters are shown in Table 4.5.

Parameter	Upper boundary	Lower boundary
T_{hot}	375°C	100°C
T_{cold}	300°C	50°C
p_{evap}	37.12 bar	1 bar
$\dot{n}_{ORC}$	50 kmol/h	5 kmol/h
$\dot{Q}_{rec}$	300 kW	0 kW

Table 4.4: Boundaries for simulations with toluene as organic working fluid.

Parameter	Value
$\eta_{turbine}$	0.80
$\eta_{pump,ORC}$	0.75
$\eta_{generator}$	0.97
η_{motor}	0.75
g	9.81 m/s^2
H	10 m
ΔT_{min}	20°C
T_{cond}	50°C

Table 4.5: Design and input parameters for the optimization.

The results of the optimization are shown in Table 4.6.

Parameter/variable	Basic ORC	Recuperative ORC
T_{hot}	375°C	375°C
T_{cold}	89.27°C	248.1°C
p_{evap}	37.12 bar	36.72 bar
$\dot{n}_{ORC}$	15.54 kmol/h	17.30 kmol/h
$\dot{Q}_{cool}$	217.7 kW	186.0 kW
$\dot{Q}_{rec}$	-	101.3 kW
$\dot{W}_{net}$	66.37 kW	86.76 kW
η_{ORC}	23.1%	31.3%
η_{solar}	70.9%	68.3%
η_{system}	16.4%	21.4%

Table 4.6: Optimized results by using the same design and input parameters as the reference.

Table 4.6 shows that the gain in net power output by applying the recuperative ORC is 30.7% compared to the basic ORC. The penalty for applying the recuperator is the rather large increase in T_{cold}, which decreases the efficiency of the solar cycle. However, the reward of the increased ORC efficiency is so much larger than this penalty, that the total system efficiency increases significantly.

Interestingly, the optimal temperature for T_{cold} given by the proposed model is higher than for the reference model for the basic ORC and lower than the reference model for the recuperative ORC. The explanation for this is that the optimal solution for the system is a trade-off between the solar cycle efficiency and the ORC efficiency. As the models for the solar cycle in the proposed model and the reference model are not equal, the optimal solutions will naturally also be different.

4.2.2 Redefined Design Parameters

In this case, the same boundaries as in Table 4.4 were used. The design and input parameters are also the same as in Table 4.5, with the exception of ΔT_{min} and T_{cond}, which are assumed to be 10°C and 40°C, respectively. The result of the optimization is shown in Table 4.7.

Parameter/variable	Basic ORC	Recuperative ORC
T_{hot}	375°C	375°C
T_{cold}	56.46°C	230.7°C
p_{evap}	37.12 bar	35.99 bar
$\dot{n}_{ORC}$	15.29 kmol/h	17.05 kmol/h
$\dot{Q}_{cool}$	215.4 kW	179.3 kW
$\dot{Q}_{rec}$	-	114.0 kW
$\dot{W}_{net}$	70.47 kW	94.43 kW
η_{ORC}	24.3%	33.9%
η_{solar}	71.4%	68.6%
η_{system}	17.4%	23.3%

Table 4.7: Optimized results with redefined input parameters.

Table 4.7 shows that all the efficiencies increase compared to the previous case. Naturally, this results in higher net power outputs for both the basic and the recuperative ORC, as the available energy from the sun remains the same for both cases. Here, the reward for applying the recuperator is an increase in net power output of 34%. Compared to the original design parameters, the net power increases with 6.2% and 8.8% for the basic and recuperative configuration, respectively. In total, the recuperative ORC benefits the most from these changes.

The effect of lowering the minimum approach temperature and the condensation temperature of the ORC is mainly that it allows the HTF of the solar cycle to heat the ORC working fluid to higher temperatures in the evaporator. The effect of the recuperator is also increased. As the condensation temperature is lowered, and the turbine outlet temperature is increased, the recuperator can transfer more heat due to the overall increased temperature difference.

4.3 Efficiency of the Solar Collector

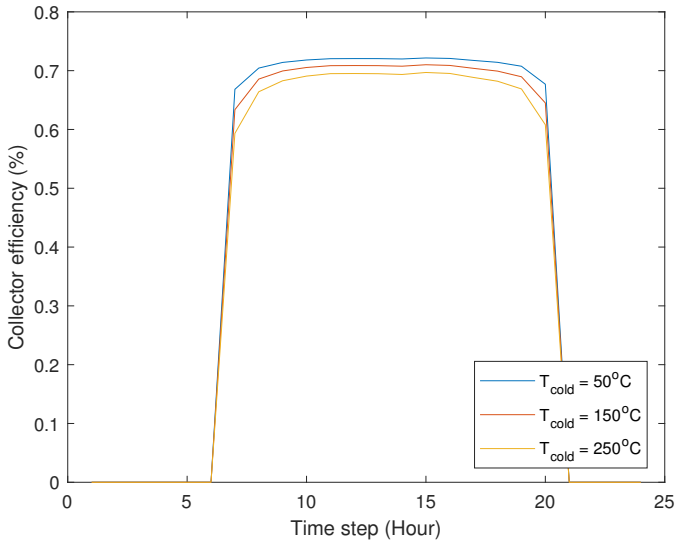

Figure 4.2: Collector efficiency for T_{hot} = 375°C.

Figure 4.2 shows the efficiency of the solar collector as it varies throughout the day. We can see how the efficiency decreases as the temperature difference between the hot and the cold HTF decreases. In Figure 4.3, this is further illustrated, showing the average collector efficiency through the day as a function of the cold HTF temperature.

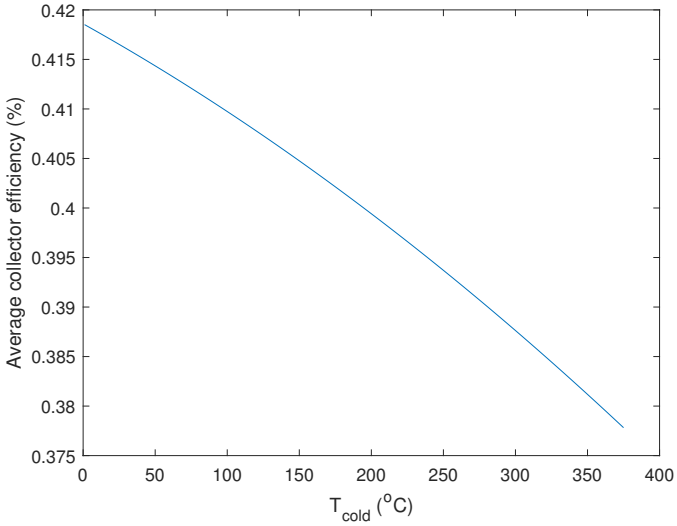

Figure 4.3: Average collector efficiency for T_{hot} = 375°C.

Considering that there are no losses in the solar cycle, except for those related to the collector efficiency, Figure 4.2 and Figure 4.3 also shows the efficiency of the entire solar cycle as a function of the hot and cold HTF temperatures.

4.4 Effects of the Organic Working Fluid

In addition to toluene, the optimized results for three other fluids were also found. The design and input parameters remain the same as those shown in Table 4.5. The boundaries also remain the same as those in Table 4.4, with the exception of the evaporation pressure upper boundary, which is set to 90% of the critical pressure of the working fluid used in the optimization.

The working fluids used for optimization and their properties are shown in Table 4.8

Working fluid	T_{crit}	p_{crit}	**Molar mass**
Toluene	319°C	41.3 bar	92.14 kg/kmol
Ethylbenzene	344°C	36.1 bar	106.2 kg/kmol
Benzene	298°C	48.8 bar	78.11 kg/kmol
Cyclohexane	280°C	40.7 bar	84.16 kg/kmol

Table 4.8: Selected fluids and their properties (Bao and Zhao, 2013).

The fluids shown in Table 4.8 were selected based on the assumption that fluids with high critical temperatures give high ORC efficiencies (Bruno et al., 2008). These fluids

have also proven to be efficient for similar models (Bruno et al., 2008; Desai and Bandyopadhyay, 2016; Tzivanidis et al., 2016)

The results of the optimization of both the basic and the recuperative ORC are shown in Table 4.9.

Working fluid	ORC type	T_{hot} (°C)	T_{cold} (°C)	p_{evap} (bar)	$\dot{W}_{net}$ (kW)	η_{ORC} (%)	η_{system} (%)
Toluene	Basic	375.0	56.46	37.12	70.47	24.3	17.4
	Rec.	375.0	230.7	35.99	94.43	33.9	23.3
Ethylbenzene	Basic	375.0	97.78	31.5	68.63	23.9	16.9
	Rec.	375.0	259.1	24.45	95.92	34.7	23.7
Benzene	Basic	366.7	59.54	43.29	69.47	24.0	17.1
	Rec.	375.0	204.7	42.93	91.84	32.8	22.6
Cyclohexane	Basic	331.1	60.2	36.63	61.85	21.2	15.5
	Rec.	375.0	230.0	36.63	92.98	33.4	22.9

Table 4.9: Optimized results for the different working fluids and ORC configurations.

Table 4.9 shows that ethylbenzene is the working fluid that gives the highest net power output with the set design and input parameters for the recuperative ORC. This is consistent with the findings of other authors optimization of the ORC, such as the findings by Cao et al. (2016). Naturally, with the highest net power output, ethylbenzene also has the highest system efficiency for the recuperative ORC. For the basic ORC, however, toluene has the highest power output and efficiency among the investigated fluids. For the recuperative ORC, there appears to be a link between the molar mass and the efficiency of the ORC. The higher the molar mass, the higher the efficiency. Of course, with respect to the optimization of the model, the different working fluids are not operating under the same conditions as each other. In addition to the limited number of fluids tested, the conclusion that that higher molar mass leads to higher ORC efficiency can not be drawn with complete certainty. However, the same connection between molar mass and ORC efficiency has also been discussed by Harinck et al. (2009), among others.

It can also be observed from Table 4.9 that the system efficiency is dominated by the efficiency of the ORC. This is especially visible for the basic ORC efficiencies of ethylbenzene and benzene. The ORC efficiency is only 0.1% higher for benzene, while the system efficiency is 0.2% higher.

4.5 Effects on the Heat Transfer Fluid Mass Flow Rates

In Figure 4.4 the resulting mass flow rates of the HTF in the solar collector, $\dot{m}_c$, and in the evaporator, $\dot{m}_{HTF}$, from the system optimization using toluene as the organic working fluid are shown.

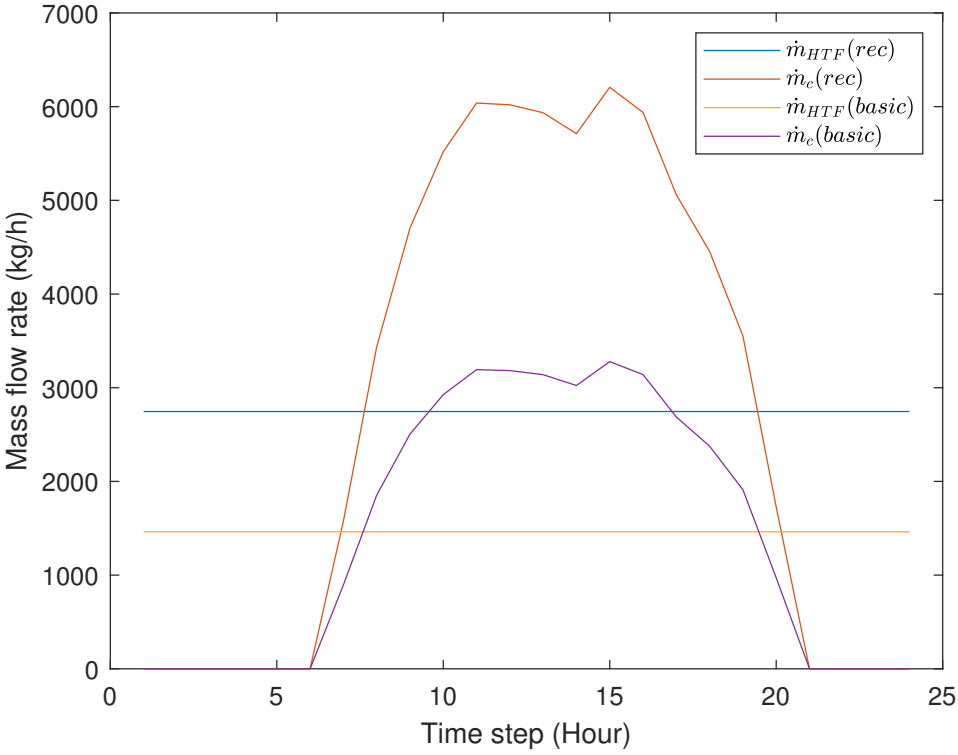

Figure 4.4: Heat transfer fluid flow rates for the basic and the recuperative ORC using toluene as the working fluid.

For the case of toluene as the working fluid, the recuperative ORC has 34% higher net power output than the basic ORC. The HTF mass flow rate to the evaporator, however, is 88% higher for the recuperative ORC. This is caused by the large decrease in temperature difference in and out of the evaporator when applying the recuperator. In turn, this will increase the needed storage capacity in the hot and cold storage tanks. The positive net flow tanks lead to an accumulation of 88% more HTF in the hot tank in the hours where the flow rate from the collector is higher than the flow rate to the evaporator. This means that the storage tanks for the recuperative ORC are required to be near twice the size needed by the basic ORC. In addition, when more HTF is stored in the tanks, the total amount of HTF in the system also increases significantly. Though the economic aspect of the system is not inside the scope of this thesis, it is evident that there is a trade-off between the investment costs and power output from the system.

Chapter 5

Conclusion and Future Work

5.1 Conclusion

The objective of this thesis was to develop a model of a solar organic Rankine cycle (SORC). The model was to be optimized to find the optimal operating conditions for maximum constant power output. Then, by running simulations, validate the performance against relevant references, and investigate the effects of varying parameters and configurations to achieve maximum constant power output.

Compared to a reference model, the modelled organic Rankine cycle (ORC) performed at similar levels for both the basic and the recuperative configuration. The comparison of the entire system model, including the solar collector and the thermal storage, was not of interest because of differences and possible errors in the reference.

The optimization of the model was done using solar data and ambient temperatures from a single day in the northwest of China. The optimized results showed that the incorporation of a recuperator in the ORC increases the efficiency and power output significantly. With toluene as the organic working fluid in the ORC, the net power output increases with 34%. However, the recuperator also decreases the temperature difference in and out of the evaporator, increasing the constant flow rate of the heat transfer fluid (HTF) with 88%. This increases the necessary size of the storage tanks and the amount of HTF needed significantly.

Toluene, ethylbenzene, benzene and cyclohexane was investigated as organic working. Among these, ethylbenzene achieved the highest power output for the given conditions with the recuperative ORC configuration. For the basic ORC configuration, toluene performed the best. For the recuperative ORC, the molar mass of the working fluid appears significant, where the results showed that the efficiency increased with increasing molar mass.

The impact of the solar collector efficiency appears to be minimal. In none of the optimization cases was it observed that a higher ORC efficiency did not coincide with higher system efficiency.

5.2 Future Work

This thesis discloses areas for SORCs that could benefit from future work, both for the proposed model and the involved technologies. The available research on SORCs operating with stable is relatively slim. This is most likely due to the heavy dependence on thermal energy storage. The storage technologies available today are either too inefficient or too expensive and immature to support steady power output.

The development of more detailed models could give a more realistic impression of the potential of SORCs with stable outputs. Another possibility is to implement different storage methods in the same system. Combining latent and sensible storage could decrease the physical size of the storage, while the effect on efficiency would have to be investigated.

Research done on ORCs operating at medium to low temperatures is readily available. Thus, the future work that is required to determine the potential of SORCs with steady power output lies in the interaction between the solar collector, thermal storage, and the ORC.

Bibliography

Aboelwafa, O., Fateen, S.-E. K., Soliman, A., Ismail, I. M., 2018. A review on solar rankine cycles: Working fluids, applications, and cycle modifications. Renewable and Sustainable Energy Reviews 82, 868–885.

AspenTech, May 2019. Milestones & innovations. https://www.aspentech.com/en/about-aspentech/milestones-and-innovations, accessed: 22.05.2019.

Ayompe, L., Duffy, A., Mc Keever, M., Conlon, M., McCormack, S., 2011. Comparative field performance study of flat plate and heat pipe evacuated tube collectors (etcs) for domestic water heating systems in a temperate climate. Energy 36 (5), 3370–3378.

Bao, J., Zhao, L., 2013. A review of working fluid and expander selections for organic rankine cycle. Renewable and sustainable energy reviews 24, 325–342.

Blanco, J., Alarcón, D., Sánchez, B., Malato, S., Maldonado, M. I., Hublitz, A., Spinnler, M., 2003. Technical comparison of different solar-assisted heat supply systems for a multi-effect seawater distillation unit. In: ISES Solar World Congress, Göteborg, Sweden, June. pp. 14–19.

Brosseau, D., Edgar, M., Kelton, J. W., Chisman, K., Ray, D., Emms, B., 2004. Testing of thermocline filler materials and molten-salt heat transfer fluids for thermal energy storage systems in parabolic trough power plants. In: ASME 2004 International Solar Energy Conference. American Society of Mechanical Engineers, pp. 587–595.

Bruno, J. C., Lopez-Villada, J., Letelier, E., Romera, S., Coronas, A., 2008. Modelling and optimisation of solar organic rankine cycle engines for reverse osmosis desalination. Applied Thermal Engineering 28 (17-18), 2212–2226.

Cao, Y., Gao, Y., Zheng, Y., Dai, Y., 2016. Optimum design and thermodynamic analysis of a gas turbine and orc combined cycle with recuperators. Energy Conversion and Management 116, 32–41.

Chen, H., Goswami, D. Y., Stefanakos, E. K., 2010. A review of thermodynamic cycles and working fluids for the conversion of low-grade heat. Renewable and sustainable energy reviews 14 (9), 3059–3067.

Chu, Y., Meisen, P., 2011. Review and comparison of different solar energy technologies. Global Energy Network Institute (GENI), San Diego, CA.

Collado, F. J., Guallar, J., 2013. A review of optimized design layouts for solar power tower plants with campo code. Renewable and Sustainable Energy Reviews 20, 142–154.

Da Cunha, J. P., Eames, P., 2016. Thermal energy storage for low and medium temperature applications using phase change materials–a review. Applied Energy 177, 227–238.

Dai, Y., Wang, J., Gao, L., 2009. Parametric optimization and comparative study of organic rankine cycle (orc) for low grade waste heat recovery. Energy Conversion and Management 50 (3), 576–582.

Desai, N. B., Bandyopadhyay, S., 2016. Thermo-economic analysis and selection of working fluid for solar organic rankine cycle. Applied Thermal Engineering 95, 471–481.

DiGenova, K. J., Botros, B. B., Brisson, J., 2013. Method for customizing an organic rankine cycle to a complex heat source for efficient energy conversion, demonstrated on a fischer tropsch plant. Applied energy 102, 746–754.

Faninger, G., 2010. The potential of solar thermal technologies in a sustainable energy future. IEA solar heating & cooling programme.

Fernández-García, A., Zarza, E., Valenzuela, L., Pérez, M., 2010. Parabolic-trough solar collectors and their applications. Renewable and Sustainable Energy Reviews 14 (7), 1695–1721.

H Abedin, A., A Rosen, M., 2011. A critical review of thermochemical energy storage systems. The open renewable energy journal 4 (1).

Hamid, M. K. A., 2007. Hysys: An introduction to chemical engineering simulation. Apostila de Hamid.

Harinck, J., Guardone, A., Colonna, P., 2009. The influence of molecular complexity on expanding flows of ideal and dense gases. Physics of fluids 21 (8), 086101.

Herrmann, U., Kelly, B., Price, H., 2004. Two-tank molten salt storage for parabolic trough solar power plants. Energy 29 (5-6), 883–893.

Kennedy, J., Eberhart, R., 1995. Particle swarm optimization (pso). In: Proc. IEEE International Conference on Neural Networks, Perth, Australia. pp. 1942–1948.

Kumar, K. R., Reddy, K., 2009. Thermal analysis of solar parabolic trough with porous disc receiver. Applied Energy 86 (9), 1804–1812.

Kuravi, S., Trahan, J., Goswami, D. Y., Rahman, M. M., Stefanakos, E. K., 2013. Thermal energy storage technologies and systems for concentrating solar power plants. Progress in Energy and Combustion Science 39 (4), 285–319.

Lambert, A., Cuevas, S., Del Río, J., 2006. Enhanced heat transfer using oscillatory flows in solar collectors. Solar energy 80 (10), 1296–1302.

Lang, C., Lee, B., 2015. Heat transfer fluid life time analysis of diphenyl oxide/biphenyl grades for concentrated solar power plants. Energy Procedia 69, 672–680.

Lee, U., Mitsos, A., 2017. Optimal multicomponent working fluid of organic rankine cycle for exergy transfer from liquefied natural gas regasification. Energy 127, 489–501.

Liu, H., Zhang, H., Yang, F., Hou, X., Yu, F., Song, S., 2017. Multi-objective optimization of fin-and-tube evaporator for a diesel engine-organic rankine cycle (orc) combined system using particle swarm optimization algorithm. Energy Conversion and Management 151, 147–157.

Macchi, E., Astolfi, M., 2016. Organic Rankine cycle (ORC) power systems: technologies and applications. Woodhead Publishing.

Mahlia, T., Saktisahdan, T., Jannifar, A., Hasan, M., Matseelar, H., 2014. A review of available methods and development on energy storage; technology update. Renewable and Sustainable Energy Reviews 33, 532–545.

Markvart, T., Bogus, K., 2000. Solar electricity. Vol. 6. John Wiley & Sons.

Mavrou, P., Papadopoulos, A. I., Stijepovic, M. Z., Seferlis, P., Linke, P., Voutetakis, S., 2015. Novel and conventional working fluid mixtures for solar rankine cycles: Performance assessment and multi-criteria selection. Applied Thermal Engineering 75, 384–396.

McMahan, A. C., 2006. Design & optimization of organic rankine cycle solar-thermal powerplants. Master's thesis, University of Wisconsin, Madison.

Moler, C., May 2004. The origins of matlab. https://se.mathworks.com/company/newsletters/articles/the-origins-of-matlab.html, accessed: 22.05.2019.

Morin, G., Dersch, J., Platzer, W., Eck, M., Häberle, A., 2012. Comparison of linear fresnel and parabolic trough collector power plants. Solar Energy 86 (1), 1–12.

Nasri, Z., Binous, H., 2009. Applications of the peng–robinson equation of state using matlab. Chemical Engineering Education 43 (2), 1–10.

NREL, U. D. o. E., May 2017. Andasol-1. https://solarpaces.nrel.gov/andasol-1, accessed: 22.05.2019.

Orosz, M., Dickes, R., 2017. Solar thermal powered organic rankine cycles. In: Organic Rankine Cycle (ORC) Power Systems. Elsevier, pp. 569–612.

Pandey, K. M., Chaurasiya, R., 2017. A review on analysis and development of solar flat plate collector. Renewable and Sustainable Energy Reviews 67, 641–650.

Pelay, U., Luo, L., Fan, Y., Stitou, D., Rood, M., 2017. Thermal energy storage systems for concentrated solar power plants. Renewable and Sustainable Energy Reviews 79, 82–100.

Peng, D.-Y., Robinson, D. B., 1976. A new two-constant equation of state. Industrial & Engineering Chemistry Fundamentals 15 (1), 59–64.

Quoilin, S., 2011. Sustainable energy conversion through the use of organic rankine cycles for waste heat recovery and solar applications. Ph.D. thesis, University of Liège, Liège, Belgium.

Rayegan, R., Tao, Y., 2011. A procedure to select working fluids for solar organic rankine cycles (orcs). Renewable Energy 36 (2), 659–670.

Sabiha, M., Saidur, R., Mekhilef, S., Mahian, O., 2015. Progress and latest developments of evacuated tube solar collectors. Renewable and Sustainable Energy Reviews 51, 1038–1054.

Safarian, S., Aramoun, F., 2015. Energy and exergy assessments of modified organic rankine cycles (orcs). Energy Reports 1, 1–7.

Schuster, A., Karl, J., Karellas, S., 2007. Simulation of an innovative stand-alone solar desalination system using an organic rankine cycle. International Journal of Thermodynamics 10 (4), 155.

Sharma, S. D., Sagara, K., 2005. Latent heat storage materials and systems: a review. International Journal of Green Energy 2 (1), 1–56.

Steinhagen, H. M., Trieb, F., 2004. Concentrating solar power, a review of the technology. Ingenia 18, 43–50.

Sunny, A., Solomon, P., Aparna, K., 2016. Syngas production from regasified liquefied natural gas and its simulation using aspen hysys. Journal of Natural Gas Science and Engineering 30, 176–181.

Tchanche, B. F., Papadakis, G., Lambrinos, G., Frangoudakis, A., 2009. Fluid selection for a low-temperature solar organic rankine cycle. Applied Thermal Engineering 29 (11-12), 2468–2476.

Tian, Y., Zhao, C.-Y., 2013. A review of solar collectors and thermal energy storage in solar thermal applications. Applied energy 104, 538–553.

Tzivanidis, C., Bellos, E., Antonopoulos, K. A., 2016. Energetic and financial investigation of a stand-alone solar-thermal organic rankine cycle power plant. Energy conversion and management 126, 421–433.

Yang, J., Li, J., Yang, Z., Duan, Y., 2019. Thermodynamic analysis and optimization of a solar organic rankine cycle operating with stable output. Energy Conversion and Management 187, 459–471.

Yang, Z., Garimella, S. V., 2010. Thermal analysis of solar thermal energy storage in a molten-salt thermocline. Solar energy 84 (6), 974–985.

Yu, H., 2016. Process integration and optimization of organic rankine cycles (orcs) for low-temperature waste heat recovery. PhD dissertation, China University of Petroleum, Beijing.

Yu, H., Feng, X., Wang, Y., 2016. Working fluid selection for organic rankine cycle (orc) considering the characteristics of waste heat sources. Industrial & Engineering Chemistry Research 55 (5), 1309–1321.

Appendix A

A.1 Basic ORC MATLAB Code

control.m:

```
hysys = actxserver ('HYSYS.Application');
hyCase = hysys.ActiveDocument;
hysolver = hyCase.Solver;
hyf=hyCase.Flowsheet;

x0=[30    15   300    7100]; % Initial values
LB=[1;       5;    100;   50]; % upper boundaries
UB=[37.12; 50;    375;   300]; %upper boundaries


options = optimoptions('particleswarm','SwarmSize',50,'
    HybridFcn',@fmincon,'FunctionTolerance', 1e-5,'Display',
     'iter' );


options.InitialSwarmMatrix = x0;
options = optimoptions(options,'MaxIterations',200);

% hyf.MaterialStreams.Item('LNG5').PressureValue = 6*100; %
     [kpa] % 600, 2500, 3000, 7000
main_sto_6;

hysys = actxserver ('HYSYS.Application');
hyCase = hysys.ActiveDocument;
hysolver = hyCase.Solver;
hyf=hyCase.Flowsheet;
```

Obj_sto_6.m:

```
function Power= Obj_sto_6(x)


    global count_num
    count_num = count_num +1;
    global RESULT6
    Error = 0;
    tic


hysys = actxserver ('HYSYS.Application');
hyCase = hysys.ActiveDocument;
hysolver = hysys.ActiveDocument.Solver;
hyf=hyCase.Flowsheet;


hysolver.Cansolve=1;



hyf.MaterialStreams.Item('ORC2').PressureValue = x(1)*100;
    % [kpa]
hyf.MaterialStreams.Item('ORC1').MolarFlowValue = x(2)
    /3600; % [kmol/s]



hysolver.Cansolve=1;

ac = 1000; %collector aperture area



hyf.MaterialStreams.Item('hotoil').TemperatureValue = x(3);
hyf.MaterialStreams.Item('hotoil2').TemperatureValue = x(4)
    ;


DNI = [0 0 0 0 0 0 266 522 696 808 879 876 864 833 901 864
    743 660 536 285 0 0 0 0];
Tam = [16.8 16 15.6 15.1 14.7 14.6 15.2 16.3 17.9 19.4 20.9
     22.1 23.1 23.9 24.3 24.5 24.4 23.7 22.8 21.6 20.2 19.1
    17.9 16.8];
```

```
38
39 massFlow = zeros(1,24); %creating an empty array for mass
       flow
40 massAcc = zeros(1,24); %creating an empty array for
       accumulated mass
41 efficiency = zeros(1,24); %creating an empty array for
       accumulated mass
42 heatload = zeros(1,24); %creating an empty array for
       accumulated mass
43
44 for i = 1:length(DNI)
45     if DNI(i)==0
46         efficiency(i)=0;
47     elseif x(4)>=x(3)
48             break;
49     else
50         efficiency(i)=0.75-0.000045*((x(3)+x(4))/2-Tam(i))
               -0.039*((x(3)+x(4))/2-Tam(i))/DNI(i)-0.0003*DNI(
               i)*(((x(3)+x(4))/2-Tam(i))/DNI(i))^2;
51     end
52     massFlow(i) = (ac*DNI(i)*efficiency(i))/((3.3811*((x(3)
           +x(4))/2)+1509.7)*(x(3)-x(4)));
53     massAcc(i) = massFlow(i)*3600;
54     heatload(i)= ac*DNI(i)*efficiency(i);
55 end
56 averageheatload=sum(heatload)/24;
57
58 s=sum(massAcc);
59 y= sum(massAcc)/(24*3600);
60 %disp(x(5));
61
62 hyf.MaterialStreams.Item('hotoil').MassFlowValue = y; % [kg
       /s]
63
64
65
66
67
68 % constraints
69
70 try
71
72
73     const(1)=hyf.MaterialStreams.Item('ORC4').
           VapourFractionValue;% turbine outlet vapor
```

```
        constraint
74      const(2)=hyf.MaterialStreams.Item('ORC1').
            VapourFractionValue;% pump inlet vapor constraint
75      const(3)=hyf.MaterialStreams.Item('ORC3').
            VapourFractionValue;% turbing inlet vapor constraint
76      const(6)=hyf.Operations.Item('E-104').
            MinimumApproachValue; % fluegas recovery heater
            minimum approach temperature constraint
77
78
79      if (const(1)<0.95||const(2)>0||const(3)<1||const(4)<20)
80          Power=10e5;
81          Error = 1; % constraint violated
82          cpu_time = toc;
83          RESULT6(count_num,:) = [Error cpu_time x Power
                averageheatload s];
84          save('RESULT6','RESULT6');
85          return
86      else
87          Error=0; % feasible
88          cpu_time = toc;
89          Power=-(hyf.Operations.Item('OptimizerSpreadsheet')
                .Cell('C1').CellValue); %[kW]
90          RESULT6(count_num,:) = [Error cpu_time x Power
                averageheatload s];
91          save('RESULT6','RESULT6');
92      end
93
94
95
96
97
98  catch exeption
99
100     Power=10e10;
101     Error=2; %infeasible
102     cpu_time = toc;
103
104     RESULT6(count_num,:) = [Error cpu_time x Power
            averageheatload s];
105     save('RESULT6','RESULT6');
106     return
107 end
```

main_sto_6.m:

```
1
2 global count_num
3 global RESULT6
4 RESULT6 = [];
5 count_num = 0;
6
7 [x,fval,exitflag,output]= particleswarm(@Obj_sto_6,4,LB,UB,
      options)
```

A.2 Recuperative ORC MATLAB Code

control.m:

```
hysys = actxserver ('HYSYS.Application');
hyCase = hysys.ActiveDocument;
hysolver = hyCase.Solver;
hyf=hyCase.Flowsheet;

x0=[30    17.3012   350   100   90]; % initial values

LB=[1;       5;    100;   50;  0]; %lower boundaries
UB=[337.12; 50;    375;   300;  300]; %upper boundaries


options = optimoptions('particleswarm','SwarmSize',50,'
    HybridFcn',@fmincon,'FunctionTolerance', 1e-5,'Display',
     'iter' );

options.InitialSwarmMatrix = x0;
options = optimoptions(options,'MaxIterations',200);

main_sto_6;

hysys = actxserver ('HYSYS.Application');
hyCase = hysys.ActiveDocument;
hysolver = hyCase.Solver;
hyf=hyCase.Flowsheet;
```

Obj_sto_6.m:

```
function Power= Obj_sto_6(x)


    global count_num
    count_num = count_num +1;
    global RESULT6
    Error = 0;
    tic


hysys = actxserver ('HYSYS.Application');
hyCase = hysys.ActiveDocument;
hysolver = hysys.ActiveDocument.Solver;
hyf=hyCase.Flowsheet;


hysolver.Cansolve=1;


hyf.MaterialStreams.Item('ORC2').PressureValue = x(1)*100;
    % [kpa]

hyf.MaterialStreams.Item('ORC1').MolarFlowValue = x(2)
    /3600; % [kmol/s]

hysolver.Cansolve=1;

ac = 1000; %collector aperture area


hyf.MaterialStreams.Item('hotoil').TemperatureValue = x(3);
     % [kmol/s]

hyf.MaterialStreams.Item('hotoil2').TemperatureValue = x(4)
    ; % [kmol/s]

hyf.Operations.Item('E-101').Specifications.Item('E-101
    ExchSpec').GoalValue=x(5);% [kW]


DNI = [0 0 0 0 0 0 266 522 696 808 879 876 864 833 901 864
    743 660 536 285 0 0 0 0];
Tam = [16.8 16 15.6 15.1 14.7 14.6 15.2 16.3 17.9 19.4 20.9
```

```
    22.1 23.1 23.9 24.3 24.5 24.4 23.7 22.8 21.6 20.2 19.1
    17.9 16.8];

massFlow = zeros(1,24); %creating an empty array for mass
    flow
massAcc = zeros(1,24); %creating an empty array for
    accumulated mass
efficiency = zeros(1,24); %creating an empty array for
    accumulated mass
heatload = zeros(1,24); %creating an empty array for
    accumulated mass

for i = 1:length(DNI)
    if DNI(i)==0
        efficiency(i)=0;
    elseif x(4)>=x(3)
            break;
    else
        efficiency(i)=0.75-0.000045*((x(3)+x(4))/2-Tam(i))
            -0.039*((x(3)+x(4))/2-Tam(i))/DNI(i)-0.0003*DNI(
            i)*(((x(3)+x(4))/2-Tam(i))/DNI(i))^2;
    end
    massFlow(i) = (ac*DNI(i)*efficiency(i))/((3.3811*((x(3)
        +x(4))/2)+1509.7)*(x(3)-x(4)));
    massAcc(i) = massFlow(i)*3600;
    heatload(i)= ac*DNI(i)*efficiency(i);
end
averageheatload=sum(heatload)/24;

s=sum(massAcc);
y= sum(massAcc)/(24*3600);



hyf.MaterialStreams.Item('hotoil').MassFlowValue = y; % [g/
    s]


% constraints

try

    const(1)=hyf.MaterialStreams.Item('ORC4').
        VapourFractionValue;% turbine outlet vapor
        constraint
```

```
71      const(2)=hyf.MaterialStreams.Item('ORC1').
            VapourFractionValue;% pump inlet vapor constraint
72      const(3)=hyf.MaterialStreams.Item('ORC3').
            VapourFractionValue;% turbing inlet vapor constraint
73      const(4)=hyf.Operations.Item('E-104').
            MinimumApproachValue; % fluegas recovery heater
            minimum approach temperature constraint
74      const(5)=hyf.Operations.Item('E-101').
            MinimumApproachValue; % fluegas recovery heater
            minimum approach temperature constraint
75
76      if (const(1)<0.95||const(2)>0||const(3)<1||const(4)
            <10||const(5)<10)
77          Power=10e5;
78          Error = 1; % constraint violated
79          cpu_time = toc;
80          RESULT6(count_num,:) = [Error cpu_time x Power
                averageheatload s];
81          save('RESULT6','RESULT6');
82          return
83      else
84          Error=0; % feasible
85          cpu_time = toc;
86          Power=-(hyf.Operations.Item('OptimizerSpreadsheet')
                .Cell('C1').CellValue); %[kW]
87          RESULT6(count_num,:) = [Error cpu_time x Power
                averageheatload s];
88          save('RESULT6','RESULT6');
89      end
90
91
92  catch exception
93
94      Power=10e10;
95      Error=2; %infeasible
96      cpu_time = toc;
97
98      RESULT6(count_num,:) = [Error cpu_time x Power
            averageheatload s];
99      save('RESULT6','RESULT6');
100     return
101 end
```

main_sto_6.m:

```
1
2 global count_num
3 global RESULT6
4 RESULT6 = [];
5 count_num = 0;
6
7 [x,fval,exitflag,output]= particleswarm(@Obj_sto_6,5,LB,UB,
      options)
```

Appendix B

B.1 HYSYS Flowsheets

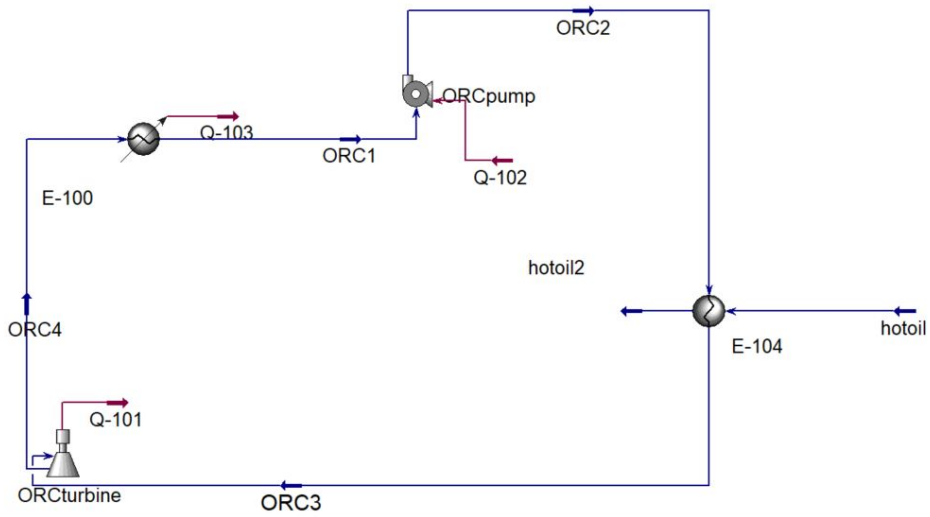

Figure B.1: Flowsheet of the basic ORC modelled in HYSYS.

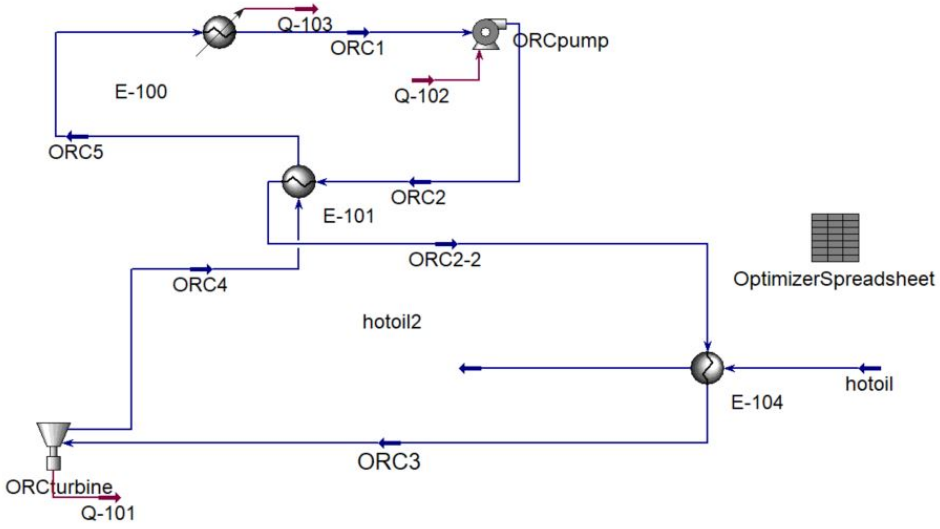

Figure B.2: Flowsheet of the recuperative ORC modelled in HYSYS.

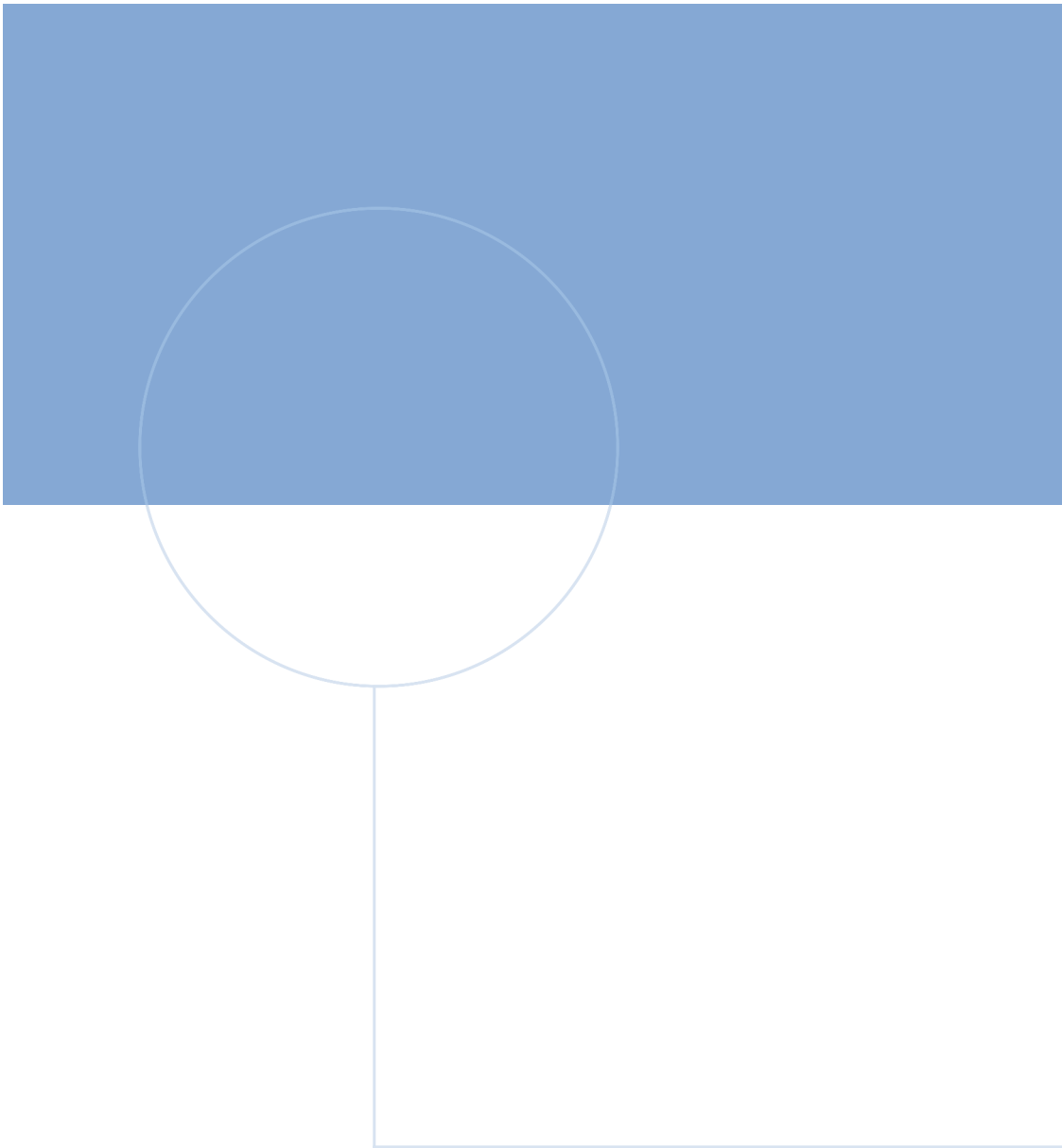

NTNU
Norwegian University of
Science and Technology